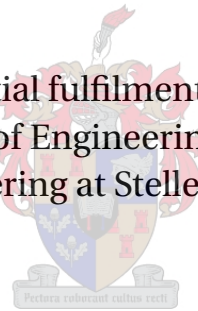


EVALUATION AND MODIFICATION OF AIR-COOLED HEAT EXCHANGER HEADER BOX DESIGN PROCEDURE

Wilhelm André Beyers

Thesis presented in partial fulfilment of the requirements for the degree of Master of Engineering (Mechanical) in the Faculty of Engineering at Stellenbosch University



Supervisor: Prof G Venter

December 2014

Declaration

By submitting this thesis electronically, I declare that the entirety of the work contained therein is my own, original work, that I am the sole author thereof (save to the extent explicitly otherwise stated), that reproduction and publication thereof by Stellenbosch University will not infringe any third party rights and that I have not previously in its entirety or in part submitted it for obtaining any qualification.

Signature:

W A Beyers

Date:
2014/09/12

Copyright © 2014 Stellenbosch University
All rights reserved.

Abstract

EVALUATION AND MODIFICATION OF AIR-COOLED HEAT EXCHANGER HEADER BOX DESIGN PROCEDURE

W A Beyers

*Department of Mechanical and Mechatronic Engineering,
University of Stellenbosch,
Private Bag X1, Matieland 7602, South Africa.*

Thesis: MEng (Mech)

December 2014

The purpose of the heat exchanger header box is to act as a high pressure manifold that redistributes process fluid from a central source to a bundle of finned tubes where it can be cooled. South African law requires that pressure vessels like this one must to be designed according to a pressure vessel design code, such as the American Society of Mechanical Engineers' (ASME) pressure vessel design code.

The two most commonly used header box designs are a plug type and a cover type header box. For the design of a plug type header box, ASME Section VIII Division 1 provides a full complement of rules and formulae necessary for producing a satisfactory pressure vessel design. Such a set of rules and formulae are however not available for cover type header boxes.

To overcome this problem, industrial manufactures have developed in-house design codes focussing specifically on the design of cover type header boxes. These in-house codes draw in part on existing formulae in the ASME code, but rely primarily on calculating the strength of a header box using a simplified model consisting of simply supported beams, each simulating a different part of the header box.

Recently there has been some concern regarding the accuracy and validity of these in-house design codes. This project has sought to address some of these concerns by evaluating one such in-house design code and comparing its results with those from finite element analyses.

For the purpose of this comparison it is shown that the header box's structure can be simplified to a representative 2D finite element model while still yielding trustworthy results. The results from the comparisons with these 2D models showed that the in-house methods produced non-conservative estimations for certain stresses in a header box. However, after analysing multiple sample designs, it was also found that header boxes that had been designed using this method were all substantially over-designed.

Two major contributing factors that lead to this over design were identified. The first was that material and manufacturing constraints frequently necessitate that material thicknesses be increased. The second factor was that because of the concern linked to the validity of these in-house design methods, designers are inclined to further increase the material thicknesses to account for any uncertainty.

To address this problem, a new 2D finite element software package was developed, on an open source platform, to accurately analyse the structure of cover type header boxes. The software is designed to integrate directly with the platform currently being used to perform the calculations for the in-house code and includes an optimiser that takes the material and manufacturing constraints into account. The software can be used to validate any existing designs, as well as providing optimal designs and accurate stress predictions for new header boxes, thus reducing uncertainty in the design process.

Opsomming

EVALUERING EN AANPASSING VAN LUGVERKOELDE HITTERUIER SPRUITSTUKHOUER-ONTWERPPROSEDURE

*("EVALUATION AND MODIFICATION OF AIR-COOLED HEAT EXCHANGER HEADER
BOX DESIGN PROCEDURE")*

W A Beyers

*Departement Meganiese en Megatroniese Ingenieurswese,
Universiteit van Stellenbosch,
Privaatsak X1, Matieland 7602, Suid Afrika.*

Tesis: MIng (Meg)

Desember 2014

Die doel van 'n hitteruiler spruitstukhouer is om te funksioneer as 'n hoë druk spruitstuk, wat proses vloeistof verdeel van 'n sentrale bron na 'n vinbuisbun- del, waar dit afgekoel kan word. Suid-Afrikaanse wette vereis dat hierdie tipe drukvatte ontwerp moet word volgens 'n drukvat ontwerpkode, soos dié van die "American Society of Mechanical Engineers" (ASME) se drukvatontwerpkode.

Die twee mees algemene spruitstukhouerontwerpe is 'n prop tipe en 'n deksel tipe spruitstukhouer. Vir die ontwerp van 'n prop tipe spruitstukhouer bied ASME Gedeelte VIII Afdeling 1 'n volledige stel reëls en formules wat nodig is om 'n bevredigende drukvat te ontwerp. So 'n stel reëls en formules is egter nie beskikbaar vir deksel tipe spruitstukhouers nie.

Om hierdie probleem te oorkom het industriële vervaardigers interne kodes begin ontwerp wat spesifiek fokus op die ontwerp van deksel tipe spruitstuk- houers. Hierdie interne kodes maak gedeeltelik gebruik van bestaande formu- les uit die ASME kode, maar maak hoofsaaklik staat op die berekening van die kragte en spannings van 'n houer deur 'n vereenvoudigde model van eenvoudig- ondersteunde balke wat elk 'n ander deel van die houer voorstel.

Onlangs het 'n mate van kommer begin ontstaan oor die akkuraatheid en gel- digheid van hierdie interne ontwerpskodes. Hierdie projek het gepoog om van

hierdie bekommernisse aan te spreek deur een van die interne ontwerpskodes te evalueer en die resultate met dié van eindige element analyses te vergelyk.

Vir die doel van hierdie vergelyking is dit bewys dat die spuitstukhouer se struktuur vereenvoudig kan word tot 'n verteenwoordigende 2D eindige element model en steeds geloofwaardige resultate kan lewer. Die resultate van die vergelyking tussen die 2D-modelle en interne ontwerpmetode het getoon dat die interne metodes spannings in die spuitstukhouer onkonserwatief voorspel. Terselfdertyd is daar egter ook gevind dat verskeie spuitstukhouerontwerpe wat ontwerp is volgens die interne ontwerpmetodes almal oor-ontwerp was.

Twee groot bydraende faktore wat gelei het tot hierdie oor-ontwerp is geïdentifiseer. Die eerste een was dat materiaal- en vervaardigingsbeperkings dikwels vereis dat materiaaldiktes verhoog word. Die tweede faktor was dat die kommer gekoppel aan die geldigheid van die interne metodes, ontwerpers geneig maak om materiaaldiktes verder te verhoog om enige onsekerheid uit te skakel.

Om hierdie probleem aan te spreek, is 'n nuwe 2D eindige element sagteware pakket ontwikkel op 'n oopbron platform, wat die struktuur van deksel tipe spuitstukhouers akkuraat ontleed. Die sagteware is ontwerp om direk te integreer met die platform wat tans gebruik word om die berekeninge vir die interne ontwerpkode te doen en sluit 'n optimeerder in wat die materiaal- en vervaardigingsbeperkings in ag neem. Die sagteware kan gebruik word om enige bestaande ontwerpe geldig te verklaar, en ook om optimale ontwerpe en akkurate spannings te voorspel vir nuwe houers. Die gebruik van hierdie sagteware sal dus lei tot verminderde onsekerheid in die ontwerpproses.

Acknowledgements

I would like to express my sincere gratitude to the following people:

- Prof Venter for his support, knowledge and great advice.
- My family for their patience, encouragement and unwavering love.
- Prof Groenwold for sharing his knowledge and so much more.
- Mike Coats, Sadley Ackers and Lundi Dila for sharing their technical expertise with me.
- Wilhelm van Rooyen for sharing his knowledge and always being willing to help.

Dedications

*This thesis is dedicate to my parents:
Thank you for your love, guidance, support and
the endless hours spent praying for me.*

Contents

Declaration	i
Abstract	ii
Opsomming	iv
Acknowledgements	vi
Dedications	vii
Contents	viii
List of Figures	xi
List of Tables	xiii
1 Introduction	1
1.1 Background	1
1.1.1 Air-cooled Heat Exchangers	1
1.1.2 Header Boxes	3
1.2 Motivation	5
1.3 Literature	6
1.4 Objectives	6
1.5 Scope	7
1.6 Overview	7
2 Current Header Box Design Methods	8
2.1 Design Code And Standards	8
2.2 Current Practice	9
2.2.1 Overview	9
2.2.2 Dimensions	10
2.2.3 Bolt Loading	12
2.2.4 Free Body Diagrams	13
2.2.5 Stress Calculations	15
2.2.6 End And Cover Plate Calculations	17

2.2.7	Information Handling And Approval	18
3	Finite Element Modelling	19
3.1	FE Model For Benchmarking	19
3.1.1	Assumptions	19
3.1.2	Boundary Conditions	20
3.1.3	Results And Comparison	22
3.2	3D Linear Model	25
3.3	3D Non-linear Model	28
3.3.1	Material Properties	28
3.3.2	Tubesheet Holes	29
3.3.3	Results	29
3.4	Discussion	32
3.5	2D Model	32
3.5.1	Boundary Conditions	33
3.5.2	Results Processing	33
4	Results and Comparison	38
4.1	2D Model Results	38
4.2	Results Comparison	41
4.3	Discussion	43
5	Proposed Solution	46
5.1	Software Structure And Components	46
5.1.1	User Interface	47
5.1.2	FE Analysis	48
5.1.3	Results Rendering	51
5.1.4	Optimisation	52
5.2	Program Validation	53
5.2.1	Model Convergence	53
5.2.2	Accuracy Test	55
6	Overall Results	57
6.1	Optimisation Potential	57
6.2	Research Impact	58
7	Conclusion and Recommendations	59
7.1	Conclusions	59
7.2	Recommendations	60
	Appendices	62
A	Geometric Details of Test Models	63
B	True Stress Strain Material Model	66

<i>CONTENTS</i>	x
C 5β-NT Element Formulation	68
D Convergence Test Plots	69
E Convergence Test Results	71
List of References	74

List of Figures

1.1	Typical Forced Draft Air-cooled Heat Exchangers Configuration (Adapted from Tubetech (n.d.))	2
1.2	Air-cooled Heat Exchanger Configurations (Hudson Product Corp., 2009)	2
1.3	Cover Type Header Box	3
1.4	Plug Type Header Box (Prinsloo, 2011)	4
1.5	Cover Type Header Box (Prinsloo, 2011)	5
2.1	Header Box Dimensions (Adapted from Prinsloo (2011))	10
2.2	Bolt Loading Free Body Diagram (Adapted from Prinsloo (2011))	13
2.3	Pressure Loading Free Body Diagram (Adapted from Prinsloo (2011)) . .	14
3.1	Bolt Loading	20
3.2	Equivalent Nozzle Pressure Loading	21
3.3	Cut Away Showing Equivalent Tubesheet Pressure Loading	21
3.4	Header Box Boundary Conditions	22
3.5	Displacement Due To Bolt Loading	23
3.6	Displacement Due To Pressure Loading	24
3.7	Header Box Planes of Symmetry	25
3.8	Header Box Quarter Model Stress Plot (0-140 MPa)	26
3.9	Header Box Quarter Model Stress Plot (0-140 MPa)	27
3.10	Header Box Quarter Model Displacement Plot (0-0.435 mm)	27
3.11	True Stress Strain Curve of Header Box Material	29
3.12	Plastic Strain Pattern of Header Box	30
3.13	Plastic Strain Pattern of Header Box	30
3.14	Plastic Strain Pattern of Header Box	31
3.15	Comparison of Plastic Strain for Sequential Load Increments	31
3.16	Header Box Without End Plate	32
3.17	2D Model Boundary Conditions	34
3.18	SCL Positions	35
3.19	Stress Linearisation Diagram (ASME, 2011)	36
4.1	Von Mises Stress Plots for 2D Finite Element Test Cases	39
4.2	Side Plate Boundary Conditions	44
4.3	Welding Detail	45

5.1	Program Structure	47
5.2	Graphical User Interface	48
5.3	Boundary Conditions	49
5.4	Stress Classification Line Positions	50
5.5	Sample Results From New FE Software	52
5.6	Results With and Without Gasket Stresses Hidden	52
5.7	Flowchart of Optimisation Search Pattern	54
5.8	Normalised Membrane Stress vs Mesh Size	55
5.9	Normalised Bending Stress vs Mesh Size	55
A.1	Test Case 1 Dimensions	63
A.2	Test Case 2 Dimensions	64
A.3	Test Case 3 Dimensions	64
A.4	Test Case 4 Dimensions	65
D.1	Test Case 1 Convergence Plots	69
D.2	Test Case 3 Convergence Plots	69
D.3	Test Case 4 Convergence Plots	70

List of Tables

3.1	Symmetric Boundary Conditions	26
3.2	Stress Classification Guide	36
4.1	2D Finite Element Model Results	40
4.2	Membrane Stress Results Comparison	41
4.3	Bending Stress Results Comparison at A1, A2 and C	42
4.4	Bending Stress Results Comparison at D	43
4.5	Bending Stress Results Comparison at B	43
5.1	Acceptance Criteria	51
5.2	Results Comparison for Test Case 1	56
5.3	Results Comparison for Test Case 2	56
5.4	Results Comparison for Test Case 3	56
5.5	Results Comparison for Test Case 4	56
6.1	Comparison of Original to Optimised Header Box Designs	57
6.2	Comparison of Original to Optimised Designs' Critical Points	58
6.3	Overall Material Reduction	58
A.1	Details Regarding Test Cases	65
E.1	Convergence Test Results for Test Case 1	71
E.2	Convergence Test Results for Test Case 2	72
E.3	Convergence Test Results for Test Case 3	72
E.4	Convergence Test Results for Test Case 4	73

Chapter 1

Introduction

The main focus of this study will be to look at and improve the methods used to design cover type header boxes for air-cooled heat exchangers. This chapter will provide background information surrounding this project, as well as motivating why this research is necessary. Finally, the objectives and the scope of the study will be given, followed by an overview of how the work was approached.

1.1 Background

1.1.1 Air-cooled Heat Exchangers

Air-cooled heat exchangers are widely used in the petrochemical, power generation and other industries where large scale process cooling is required. They are used as a means to facilitate chemical processes and increase plant efficiency. Air-cooled heat exchangers are preferred for process cooling in areas that have scarce water resources. Compared to shell and tube heat exchanges and wet cooling towers, they provide a more sustainable solution because they do not need any auxiliary water supply (GEA Rainey, n.d.).

An air-cooled heat exchanger is a device that rejects heat from a process fluid directly to ambient air (Hudson Product Corp., 2009). By construction, it is simply a pressure vessel that removes heat from a process fluid by forcing cool ambient air over a collection of finned tubes through which the fluid is flowing (GEA Rainey, n.d.). Figure 1.1 shows the typical layout of a forced draft air-cooled heat exchanger. Hot process fluid is pumped in through an inlet header box, which splits the fluid into the finned tubes. Here the water flows down the tubes and into a secondary header box chamber before exiting through an outlet or being redirected for a second pass. At the same time, cool air is blown over the finned tube bundle by a fan to accelerate the exchange of heat between the air and the fluid in the tubes.

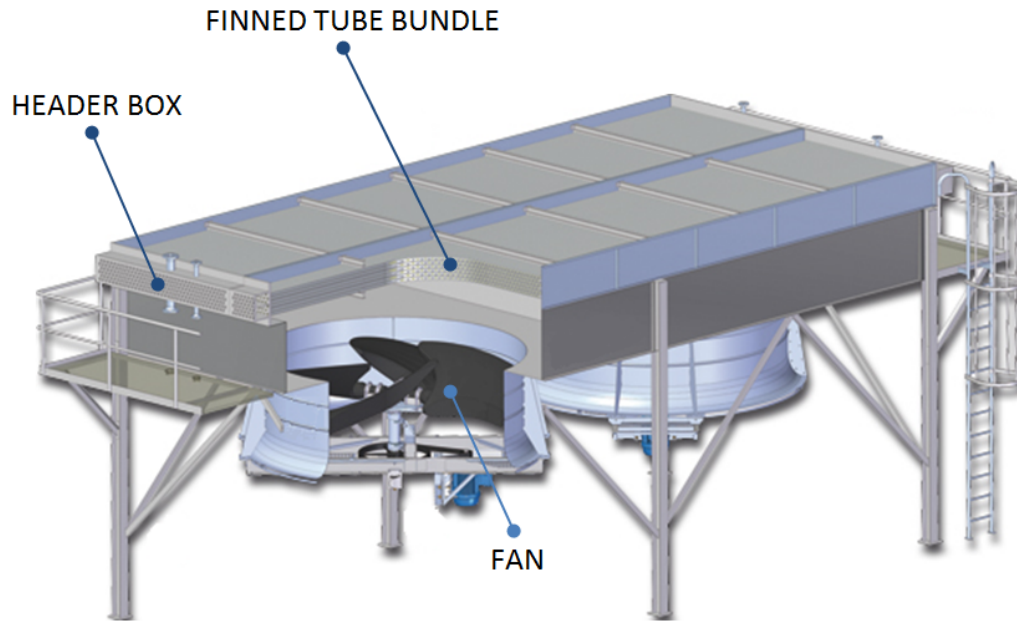


Figure 1.1: Typical Forced Draft Air-cooled Heat Exchangers Configuration (Adapted from Tubetech (n.d.))

In addition to the forced draft configuration shown in figure 1.1, where air is forced through the heat exchanger, an air-cooled heat exchangers can also be arranged in an induced draft configuration where a fan draws air over the heat exchanger unit. The two layouts are compared in figure 1.2. The figure serves to illustrate how the components of an air-cooled heat exchanger are arranged and how they interact with the header box.

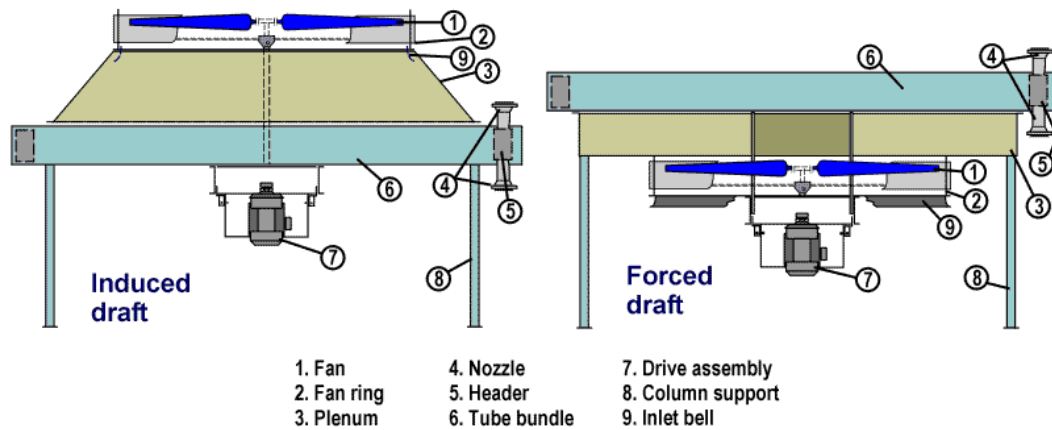


Figure 1.2: Air-cooled Heat Exchanger Configurations (Hudson Product Corp., 2009)

1.1.2 Header Boxes

The purpose of the heat exchanger header box is to act as a high pressure manifold. As for the header box shown in figure 1.3, process fluid will flow into the two large nozzles and out through the holes in the tubesheet. The two most commonly used header box designs are the removable cover and plug type header boxes.

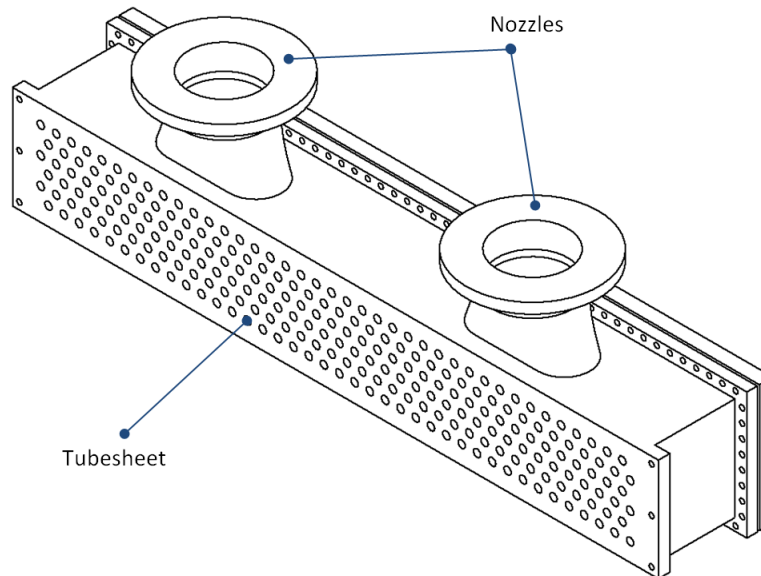


Figure 1.3: Cover Type Header Box

1.1.2.1 Plug Type Header Box

Figure 1.4 shows a diagram of the plug type header's layout. The header consists of six metal plates welded together at all the seams to form an enclosed box. For every hole drilled in the tubesheet of the box, a corresponding hole is drilled in the plug sheet. During the construction phase the plug sheet holes are used as access ports to weld the finned tubes to the tube sheet. While the box is in service each hole is fitted with a screw in plug, which can then easily be removed to gain access to the insides of the finned tubes and the header box itself for inspection and cleaning.

The benefits of the plug type header box are that, because it is welded on all sides, the structure is rigid and strong. This allows it to operate at pressure ranges exceeding 3 MPa (API, 2006). The drawback of this header box design is however that the small size of the plug holes seriously complicate inspection and cleaning of the system. This is a particular problem if the process fluid in question causes

fouling in the system, because while cleaning the tubes may still be easy, cleaning the inside of the box itself becomes very difficult.

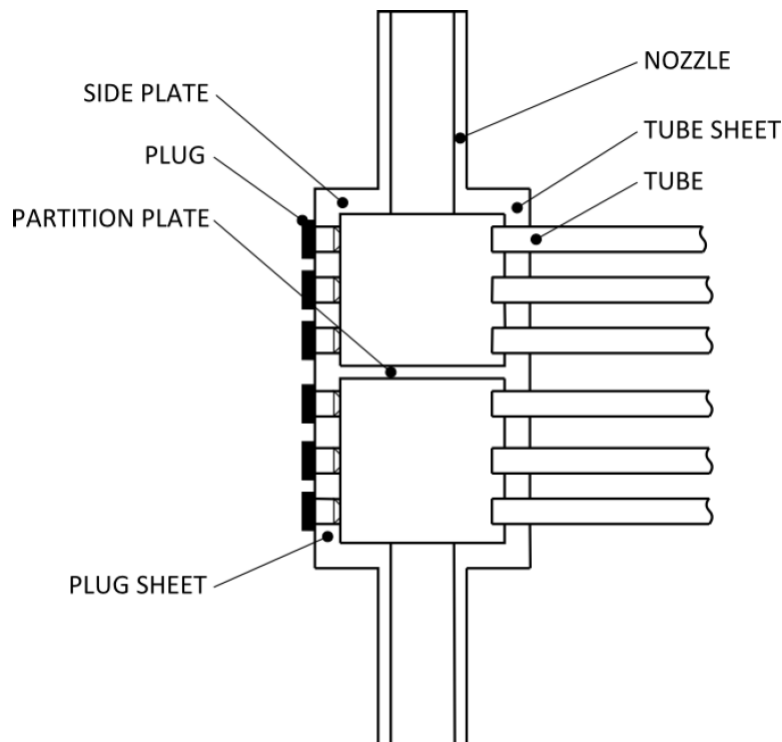


Figure 1.4: Plug Type Header Box (Prinsloo, 2011)

1.1.2.2 Cover Type Header Box

Figure 1.5 shows two cover type header box configurations. In both cases the header is made up of five metal plates welded together to form an open box. A free standing cover plate is then fastened to the frame with a flanged connection to complete the box. The only difference between the two configurations is that the tubesheet changes from being part of the welded section of the box to being integrated with the cover plate of the box.

The major benefit of this design over the plug type header box is that an entire side of the box can be removed, greatly simplifying inspection and cleaning processes. The drawback is however that because the box's design includes a flanged joint with a gasket to keep it sealed, it is less rigid compared to the welded joints of the plug type header. This limits the operational pressure range of the header box to below 3 MPa, as recommended in table A.2 of the American Petroleum Institute standard (API, 2006).

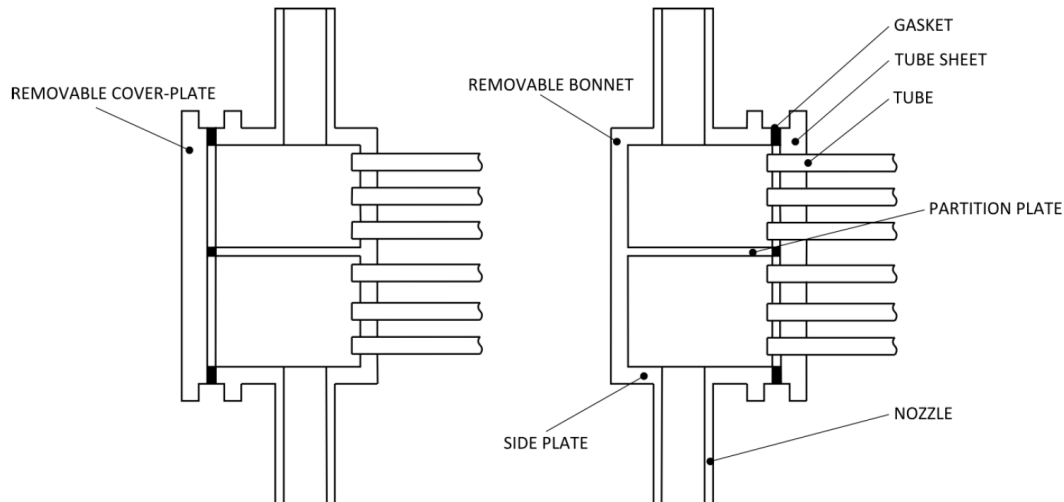


Figure 1.5: Cover Type Header Box (Prinsloo, 2011)

1.2 Motivation

When a plug type header box needs to be designed, the process is fairly simple as a full complement of the rules and formulae needed for the design are available in Division 1 of Section VIII in the ASME design code. This is not the case for cover type header boxes. Even though the code provides rules for the design of a large array of pressure vessels, the complicated geometries of the cover type header box make it very hard to describe their design requirements by a set of simple rules. For this reason, industrial manufactures have come up with in-house design codes, developed to focus specifically on the design of cover type header boxes. The codes draw primarily from ASME Section VIII, but also includes considerations from API Standard 661.

In recent years however, there has been some concern regarding the accuracy and validity of these in-house design codes. In particular, for the in-house code to be evaluated in this study, the concerns have been as follows:

- The structural effect of the forces that the flange exerts on the side plate is not analysed.
- The stress in the side plate is only analysed at its centre and at the joint where it meets the tubesheet. There is however no proof that the actual maximum stress occurs at either of these points.

To address these concerns, an industrial manufacturing partner has commissioned this study to look at the overall process of how cover type header boxes are designed and to implement improvements that will increase the credibility and accuracy of this process.

In addition to this focus, the manufacturer also stated that it had in the past commissioned finite element analyses on some of its header box designs and that in nearly all the cases the results had shown a significant degree of over design. In response to this, they have requested that this study also look at quantifying the optimisation potential in this design field.

1.3 Literature

In the past, the analysis of cover type header box design has been part of two other master's theses. One of these studies was performed by Ackers (2012). His study looked at combining the mechanical and thermal design of a cover type header box in order to improve the cost to performance ratio of these header boxes. This study used the same in-house design code to be considered in this study as the basis for its mechanical design division. However, because its primary focus was on improving the overall cost performance ratio of the header box rather than improving the mechanical design process, its content did not have such a great influence on this study.

The second masters thesis relevant to this study was conducted by Prinsloo (2011). The focus of Prinsloo's study was to evaluate multiple design methods and considerations linked to the design of cover type header boxes. As part of this study, Prinsloo compared the results of an in-house design method, similar to the one used in this study, to those of a finite element model. His results showed that the in-house design code's results held very little correlation with those predicted by the finite element model and that the in-house method predicted non-conservative results for some parts of the header box. The present study will in part also perform such an evaluation, but while Prinsloo's study was primarily focussed on the evaluation of current design practices, this study will go further to also implement improvements to the current design process and look at optimising the design process.

1.4 Objectives

1. Evaluate current design methods
2. Implement design phase changes to improve the current header box design process
3. Quantify the optimisation potential of the current header box design process

1.5 Scope

- Only cover type header boxes will be considered
- Structural support of pass partitions will not be considered
- Nozzle placement and the resulting structural effects will not be considered
- The effect of stress concentrations around individual tubesheet holes will not be considered
- Cover plate, end plate and flange design will not form part of this study as they are covered in enough detail by existing design codes

1.6 Overview

Chapter 1 provides background about this project and motivates why this research is necessary. The objectives and scope of the project is also provided.

Chapter 2 describes an in-house design code currently being used to design cover type header boxes and the regulations that it is subject to.

Chapter 3 analyses the structure of a header box using finite element methods and describes a simplified 2D finite element header box model that was developed for use in this study.

Chapter 4 compares and discusses the results from the 2D finite element model to those predicted by the design method from chapter 2.

Chapter 5 describes a new software package that was developed to analyse and optimise the design of a header box, using the 2D finite element model from chapter 3.

Chapter 6 compares a number of the optimised header box designs to their original designs, followed by a discussion of the impact that the new software will have on the future design processes for cover type header boxes.

Chapter 7 provides a conclusion to the project and recommends areas of further research.

Chapter 2

Current Header Box Design Methods

This chapter discusses the overarching requirement and common practices for designing heat exchanger header boxes. First, the design codes and standards that need to be satisfied when designing heat exchanger header boxes are explained, followed by an example of a design method used in industry.

2.1 Design Code And Standards

Under South African law (Department of Labour RSA, 2009), any vessel that operates under pressure has to be designed according to a pressure vessel design code. According to South African National Standard 347 (SABS, 2012), this is any vessel with an internal pressure exceeding 50 kPa. A widely used design code is the American Society of Mechanical Engineers (ASME) Boiler & Pressure Vessel Code Section VIII (ASME, 2011).

Division 1 of the code provides a set of rules that needs to be followed for the satisfactory design of a variety of pressure vessels. This method is known as "Design by Rule". For the case of designing a cover type header box however, the code does not provide a complete set of design requirements. Designers are instead required to design all components not covered by the code using "good engineering principles". These designs must then to be presented to an Authorised Inspection Authority for approval, in order for the design to be deemed satisfactory.

An alternative to the design by rule method is presented in Part 5 of Division 2 of the code, called Design by Analysis. The division provides guidelines of how a numerical model of a structure may be set up for analysis and how the results are to be interpreted. Various failure criteria are given for the results to be compared to in order to ensure that the design is satisfactory.

Pressure vessels are usually also designed to meet the requirements of a general standard, such as the American Petroleum Institute (API) Standard 661 (API, 2006), or those of a company specific standard if requested by a client. Instead of giving more requirements that must be followed, these standards provide guidelines and suggestions pertaining to good engineering practice in the design and construction of header boxes.

2.2 Current Practice

This section will look at an example of an in-house design code currently being used to design cover type header boxes. The information in this section was provided by the industry partner that commissioned this study.

2.2.1 Overview

Cover type header boxes have a complicated shape for which there are no analytical stress calculation formulae. Therefore, the shape of the header boxes are broken up into a collection of simple geometries and calculations are then performed on these. For this to happen a few simplifications first need to be made:

1. For the purpose of calculating the stress in the side plates and tubesheet, the stiffness of the end plates and nozzles are ignored
2. The cover plate, side plates and tubesheet are each treated as a simply supported beam
3. Holes in the tubesheet are accounted for by a perforated plate ligament efficiency factor
4. Only internal pressure and bolt loading is considered
5. Bolt-induced bending moments are applied uniformly throughout the entire structure of the header box
6. Bending moments are applied to the ends of the side plates and the tubesheet to simulate the condition that they stay at 90° to one another

2.2.2 Dimensions

The core header box dimensions are shown in figure 2.1.

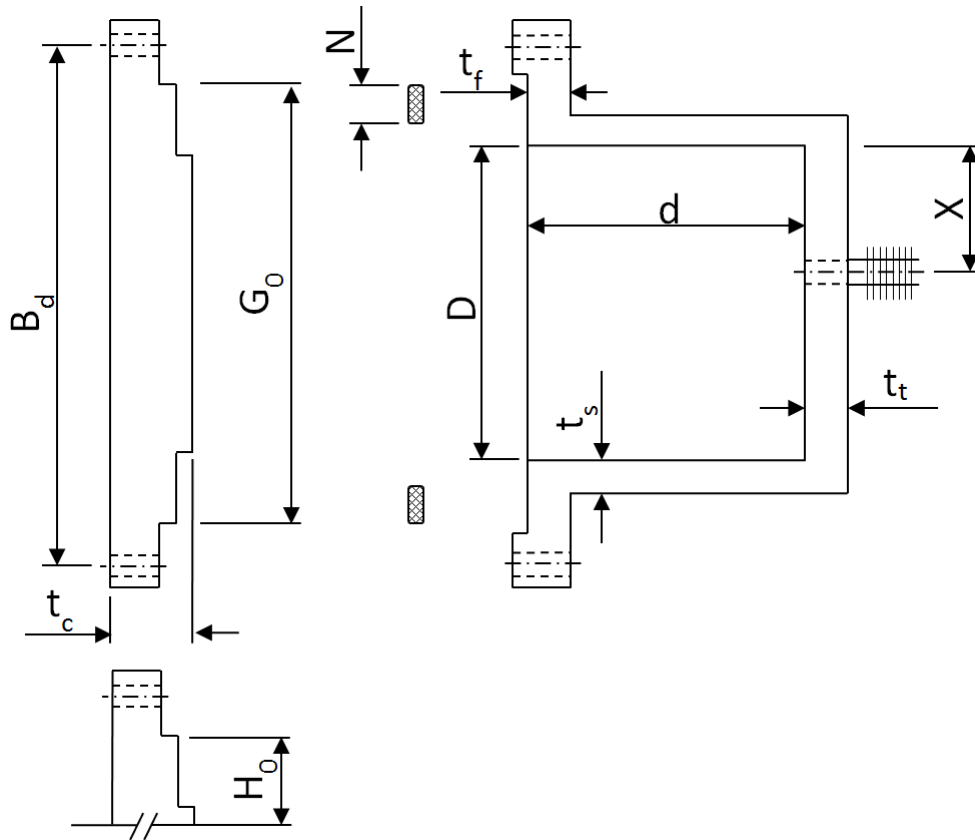


Figure 2.1: Header Box Dimensions (Adapted from Prinsloo (2011))

As required by ASME, these dimensions are modified before being used in calculations, to account for the corrosion allowance, C_a . While in operation, the interior of the header box will be exposed to corrosive fluids. The calculations account for a reduction in wall thickness by subtracting the corrosion allowance from the thickness of all the header box plates in contact with the process fluid.

The dimensions used for header box calculations in its corroded condition are given by equations (2.2.1) to (2.2.6).

Side plate thickness:

$$t_s = t_{s \text{ new}} - C_a \quad (2.2.1)$$

Tubesheet thickness:

$$t_t = t_{t \text{ new}} - C_a \quad (2.2.2)$$

Flange plate thickness:

$$t_f = t_{f_{new}} - C_a \quad (2.2.3)$$

Internal tubesheet width:

$$D_c = D - 2C_a \quad (2.2.4)$$

Header box depth:

$$d_c = d + C_a \quad (2.2.5)$$

Distance to centre-most tube row:

$$X = X + C_a \quad (2.2.6)$$

Finally, the length and width of the cover plate, H_0 and G_0 need to be modified to account for effective gasket seating width. The effective gasket seating width describes how much of the gasket will theoretically be in contact with the cover plate and flange. Table 2-5.2 in Mandatory Appendix 2 of ASME Section VIII Division 1 (2011) gives the relevant equations for calculating this width b .

First the basic seating width, b_0 , is calculated using equation (2.2.7)

$$b_0 = \frac{N}{2} \quad (2.2.7)$$

where N is the the gasket width shown in figure 2.1. Depending on the value of b_0 , b is given by equation (2.2.8) or (2.2.9).

if $b_0 \leq 6\text{mm}$

$$b = b_0 \quad (2.2.8)$$

else

$$b = 0.5C_{ul} \sqrt{\frac{b_0}{C_{ul}}} \quad (2.2.9)$$

where C_{ul} is a conversion factor for using SI units. $C_{ul} = 25.5\text{mm/inch}$.

The effective cover plate length and width are then given by equations (2.2.10) and (2.2.11) respectively.

$$H = H_0 - 2b \quad (2.2.10)$$

$$G = G_0 - 2b \quad (2.2.11)$$

2.2.3 Bolt Loading

For the header box to seal properly, the correct bolt load must be applied over the flange. If the load is too large, the gasket will be crushed and if it is too small the gasket will not seal tightly.

The minimum bolt load required during operation, that will prevent internal pressure from separating the flange connection, is given by equation 2.2.12

$$W_{m1} = PGH + 2mPb[2(G + H) + H] \quad (2.2.12)$$

where P is the internal pressure and m is the gasket factor. The minimum bolt load required to ensure adequate seating of the gasket is given by equation 2.2.13

$$W_{m2} = yb[2(G + H) + H] \quad (2.2.13)$$

where y is the gasket seating stress. m and y are obtained from Table 2-51 in Mandatory Appendix 2 of ASME Section VIII Division 1 (2011).

Based on these two bolt loading conditions, the minimum required bolt area A_m is selected as

$$A_m = \max(A_{m1}, A_{m2}) \quad (2.2.14)$$

where

$$A_{m1} = \frac{W_{m1}}{S_{bd}} \quad (2.2.15)$$

$$A_{m2} = \frac{W_{m2}}{S_{ba}} \quad (2.2.16)$$

A_{m1} and A_{m2} represent the minimum required bolt area for each loading condition with S_{bd} and S_{ba} being the allowable material stress at design and ambient temperatures respectively.

Bolt sizes are then selected such that the actual bolt area, A_b , is greater than A_m , where

$$A_b = N_b A \quad (2.2.17)$$

N_b is the number of bolts around the flange and A is the bolt area specified in Tubular Exchanger Manufacturers Association (TEMA) standard Table D-5 (TEMA, 2007).

Corresponding to the value of N_b , the bolt pitch, P_b , is checked to ensure that it is larger than the minimum values set out in Table 2 of the API standard (2006) and smaller than the maximum values prescribed by the TEMA standard (TEMA, 2007), as given by equation 2.2.18

$$P_b = 2d_b + \frac{6t_f}{m + 0.5} \quad (2.2.18)$$

where d_b is the bolt diameter.

Finally, the design bolt loading on the flange is given by equation 2.2.19

$$W_j = \frac{S_{ba}(A_m + A_b)}{2} \quad (2.2.19)$$

where the average of A_m and A_b is multiplied by the allowable stress instead of A_m alone, in order to compensate for accidental over tightening of the bolts.

2.2.4 Free Body Diagrams

For simplicity, the free body diagrams for the case of bolt loading and pressure loading are considered separately. It is important to note that from this point forward, all calculations are performed for a unit width of the header box. Figure 2.2 shows the free body diagram for bolt loading.

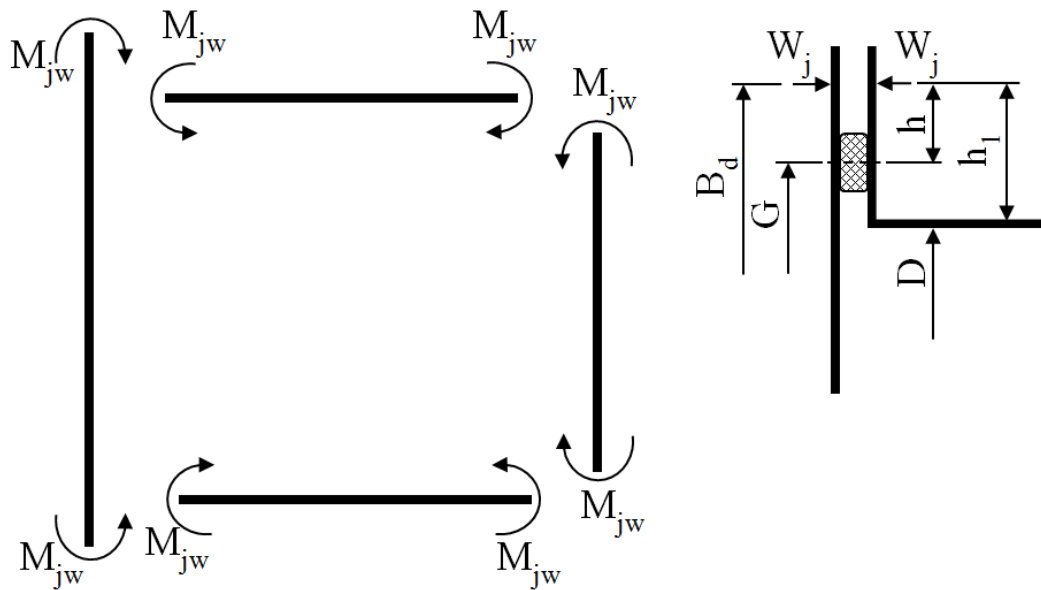


Figure 2.2: Bolt Loading Free Body Diagram (Adapted from Prinsloo (2011))

In the figure, M_{jw} represent the resulting bending moment acting on the header box walls, caused by the bolt force, F_b , acting over a portion of the flange. M_{jw} is given by equation 2.2.20.

$$M_{jw} = \frac{W_j h}{N_b P_b} \quad (2.2.20)$$

In a similar manner, the bending moment acting on the flange at the center of the gasket's effective seating area is given by equation 2.2.21.

$$M_{jf} = \frac{W_j h_1}{N_b P_b} \quad (2.2.21)$$

Figure 2.3 shows the free body diagram for the pressure loading case.

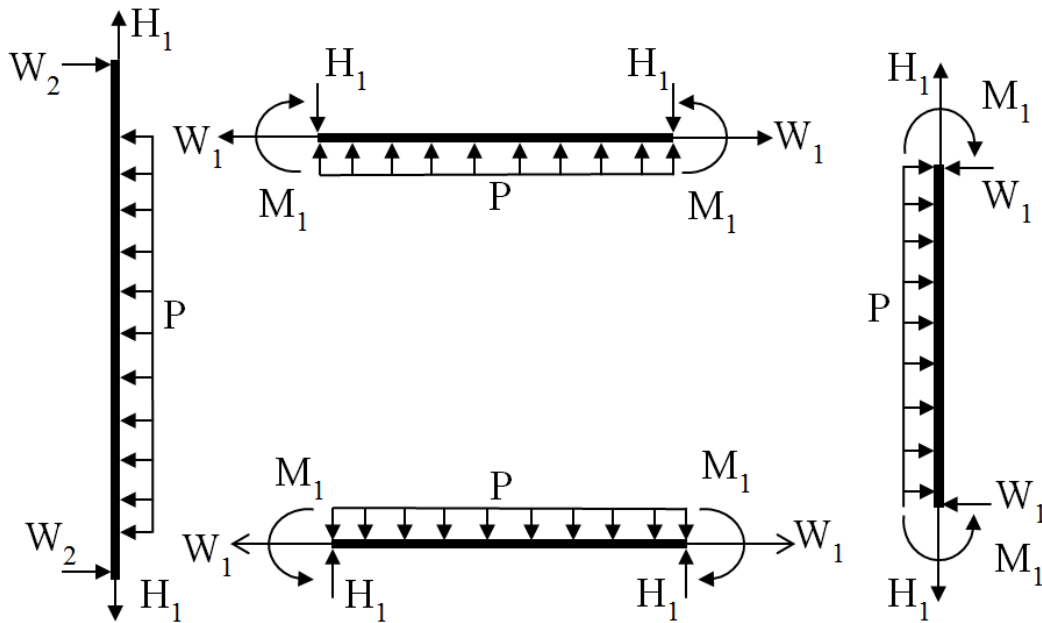


Figure 2.3: Pressure Loading Free Body Diagram (Adapted from Prinsloo (2011))

The reaction forces H_1 and W_1 are calculated using equations (2.2.22) and (2.2.23). W_2 is not calculated because it will not be used for any further calculations.

$$H_1 = \frac{Pd_c}{2} \quad (2.2.22)$$

$$W_1 = \frac{PD_c}{2} \quad (2.2.23)$$

Equation (2.2.24) gives the general equation for the bending moment at the center of a simply supported beam under uniform loading, where k is the beam length.

$$M = \frac{Pk^2}{8} \quad (2.2.24)$$

From (2.2.24), it translates that the bending moment at the center of the side plate and tubesheet is given by equations (2.2.25) and (2.2.26) respectively.

$$M_{p4} = \frac{Pd_c^2}{8} \quad (2.2.25)$$

$$M_{p8} = \frac{PD_c^2}{8} \quad (2.2.26)$$

The bending moment at the center most tube row is given by equation (2.2.27)

$$M_{px} = \frac{PX(D_c - X)}{2} \quad (2.2.27)$$

The bending moment M_1 is applied to the ends of both the side plates and tubesheet in order to simulate the joints between them staying at right angles. M_1 is calculated using equation (2.2.28)

$$M_1 = \frac{P}{24} \left(\frac{\frac{D_c^3}{I_t} + \frac{d_c^3}{I_s}}{\frac{D_c}{2I_t} + \frac{d_c}{3I_s}} \right) \quad (2.2.28)$$

where the side plate and tubesheet second moment of inertia is given by equations (2.2.29) and (2.2.30) respectively.

$$I_s = \frac{t_s^3}{12} \quad (2.2.29)$$

$$I_t = \frac{t_t^3}{12} \quad (2.2.30)$$

2.2.5 Stress Calculations

In this section, stresses at key points in the header box are calculated and compared to the relevant allowable stress. In each case, if the calculated stress is less than the allowable stress, the relevant plate thickness is acceptable.

2.2.5.1 Flange

The maximum shear stress in the flange is given by equation (2.2.31)

$$S_s = \frac{W_j}{P_b N_b t_f E_w} < \frac{S_{df}}{2} \quad (2.2.31)$$

where E_w is the joint efficiency and S_{df} is the allowable flange material stress.

Bending stress in the flange is given by equation 2.2.32.

$$S_b = \frac{6M_{jf}}{t_f^2 E_w} < 1.5S_{df} \quad (2.2.32)$$

Finally the combined stress in the flange must satisfy the criteria set out in equation 2.2.33

$$S_{comb} = \sqrt{(2S_s)^2 + S_b^2} < 1.5S_{df} \quad (2.2.33)$$

2.2.5.2 Side plate

Membrane stress in the side plate is given by equation 2.2.34

$$S_m = \frac{W_1}{t_s E_n} < S_{ds} \quad (2.2.34)$$

where E_n is the side plate efficiency, related to the nozzle holes cut in the plate and S_{ds} is the allowable material stress in the side plate

Bending stress at the center and ends of the side plate is given by equations 2.2.35 and 2.2.36 respectively.

$$S_{b4} = \frac{6(M_{p4} - M_1 + M_{jw})}{t_s^2 E_n} < 1.5S_{ds} \quad (2.2.35)$$

$$S_{b5} = \frac{6(M_1 - M_{jw})}{t_s^2 E_w} < 1.5S_{ds} \quad (2.2.36)$$

The combined stress is given by equation 2.2.37

$$S_{comb} = S_m + \max(|S_{b4}|, |S_{b5}|) < 1.5S_{ds} \quad (2.2.37)$$

2.2.5.3 Tubesheet

In order to account for the reduced load carrying capacity of the tubesheet, because it is a perforated sheet, a ligament efficiency, e , is calculated by equation 2.2.38 and applied to the relevant stress calculations.

$$e = \frac{P_t - d_1}{P_t} \quad (2.2.38)$$

P_t is the pitch and d_1 is the diameter of the holes in the tubesheet.

Membrane stress in the tubesheet is then given by equation 2.2.39

$$S_m = \frac{H_1}{t_t e} < S_{dt} \quad (2.2.39)$$

where S_{dt} is the allowable material stress in the tubesheet.

Bending stress at the center-most tube row, center and ends of the tubesheet are given by equations 2.2.40 to 2.2.42 respectively.

$$S_{b6} = \frac{6(M_{jw} + M_{px} - M_1)}{t_t^2 e} < 1.5S_{dt} \quad (2.2.40)$$

$$S_{b7} = \frac{6(M_{jw} - M_1)}{t_t^2 E_w} < 1.5S_{dt} \quad (2.2.41)$$

$$S_{b8} = \frac{6(M_{jw} + M_{p8} - M_1)}{t_t^2} < 1.5S_{dt} \quad (2.2.42)$$

The combined stress is given by equation 2.2.43

$$S_{comb} = S_m + \max(|S_{b6}|, |S_{b7}|, |S_{b8}|) < 1.5S_{dt} \quad (2.2.43)$$

2.2.6 End And Cover Plate Calculations

The end and cover plates are designed according to Section UG-34 of ASME Section VIII Division 1. This allows for the required thickness of these plates to be calculated directly, rather than having to check that all the relevant stresses in the plates are within bounds.

2.2.6.1 End Plate

The required thickness of the end plate is calculated with equation 2.2.44

$$t_{creq} = d \sqrt{\frac{ZCP}{S_{de}E_w}} + C_a \quad (2.2.44)$$

where

$$Z = \min\left(2.5, 3.4 - 2.4 \frac{d}{D}\right) \quad (2.2.45)$$

$$d = \min(d_c, D_c) \quad (2.2.46)$$

$$D = \max(d_c, D_c) \quad (2.2.47)$$

and C is an attachment factor given in figure UG-34. S_{de} is the allowable end plate material stress and E_w is the joint efficiency.

2.2.6.2 Cover plate

The required cover plate thickness is calculated with equation 2.2.48

$$t_{creq} = d \sqrt{\frac{ZCP}{S_{dc}E_w} + \frac{6W_j h}{S_{dc}E_w L d^2}} + C_a \quad (2.2.48)$$

where

$$d = G \quad (2.2.49)$$

$$D = H \quad (2.2.50)$$

$$Z = \min\left(2.5, 3.4 - 2.4 \frac{d}{D}\right) \quad (2.2.51)$$

$$L = 2(G + 2h + H + 2h) \quad (2.2.52)$$

S_{dc} is the allowable cover plate material stress.

2.2.7 Information Handling And Approval

In order to simplify the process of performing all these calculations, this manufacturer has programmed all of these equations into an Excel spreadsheet platform. This way, each time a new header box has to be designed, it is only necessary to input its dimensions and loads and the strength of the structure is automatically calculated.

When design calculations are completed, they are sent to an Authorised Inspection Authority (AIA) for approval. Once the AIA signs off on the design, the header box may be built.

Chapter 3

Finite Element Modelling

The first step in validating the current design procedure and searching for possible areas to improve the overall design process was to construct a complete finite element (FE) model of a header box. The benefit of a complete FE model is that it not only allows the user to make sure that a structure is strong enough, but also because of the visual nature of the results, helps the user understand how the structure will behave under loading.

3.1 FE Model For Benchmarking

The first header box model considered was a 3D linear FE model of a complete header box. The dimensions of the model were taken from an example case provided by an industrial manufacturer, for which an industry FE analysis report was also available. The purpose of constructing this model was to create a baseline of results which could be compared to the results of the industry report in order to establish a benchmark for the modelling techniques and assumptions to be used in this study. The geometric details of this example are provided in Appendix A as Test Case 1.

3.1.1 Assumptions

When constructing a FE model, it is not always practically possible or necessary to consider every detail that is present in the real structure. Care must however be taken to ensure that the assumptions made are either conservative or still allow for the real component to be simulated accurately. The simplifications and assumptions used for this model are:

Simplifications

- Weld geometries were not included
- The structural effect of the tubes welded to the tubesheet were ignored

Assumptions

- The gasket stays in contact with the flange and cover plate at all times
- Pressure loads within the nozzles and finned tubes can be replaced with equivalent distributed loads at the openings
- Bolts can be replaced with equivalent forces at their contact areas

These assumption are similar to those used in the industry report.

3.1.2 Boundary Conditions

As part of the FE model, various fixed displacements and loads are applied to specific points on the header box. They serve to simulate the operating conditions that the box will experience.

Bolt Loading

Modelling the exact geometry of each flange bolt would be computationally very expensive and unnecessary as the actual stress distribution within the bolt is of no value to the analysis of the header box. Instead, it was decided to represent each bolt with an equivalent distributed load couple acting on the flange and cover plate as shown in figure 3.1.

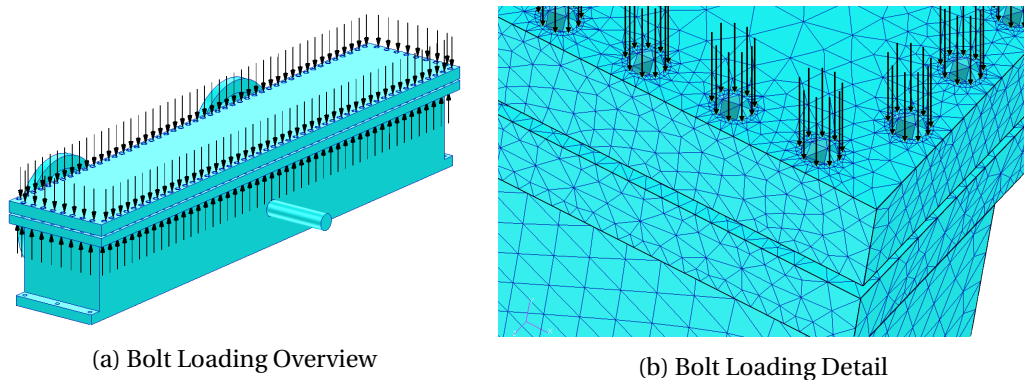


Figure 3.1: Bolt Loading

Internal Pressure

A uniform internal pressure was applied to all of the interior surfaces of the header box.

Nozzle and Tubesheet Loading

In order to account for the internal pressure load in the piping system connected to the header box, equivalent loads were applied to the nozzles and tubesheet holes. As shown in figure 3.2, the equivalent loads on the nozzles were applied as distributed loads to the outer surface of the nozzle flanges. In the case

of the tubesheet, figure 3.3 shows the equivalent loads that applied to the edge of each tubesheet hole. The individual loads were applied as a distributed edge load along the inside edge of each hole. The size of the loads are directly proportional to the internal pressure being applied to the header box and as such are calculated as the product of the relevant hole area and the internal design pressure of the header box.

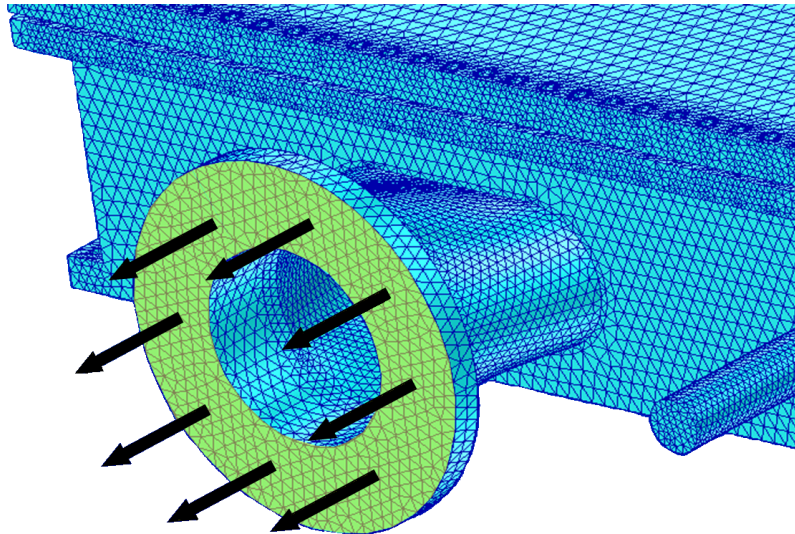


Figure 3.2: Equivalent Nozzle Pressure Loading

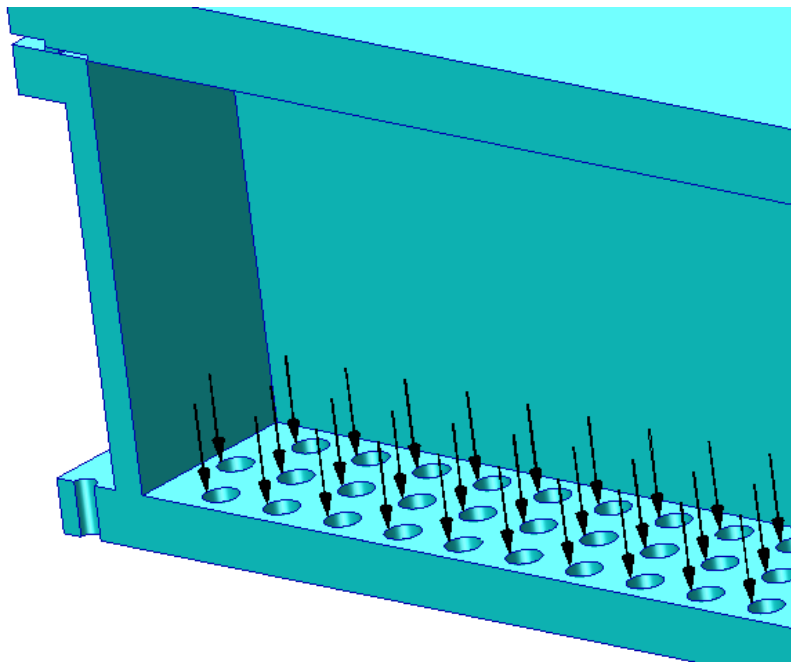


Figure 3.3: Cut Away Showing Equivalent Tubesheet Pressure Loading

Fixed Displacements

Two sets of fixed displacements were applied to the header box to simulate it being bolted to the frame of an air cooled heat exchanger. The areas marked *A* and *B* in figure 3.4 were constrained from moving in the *x* direction and the six holes lying within these areas were each constrained radially relative to their own centre line to simulate the bolts that will be used.

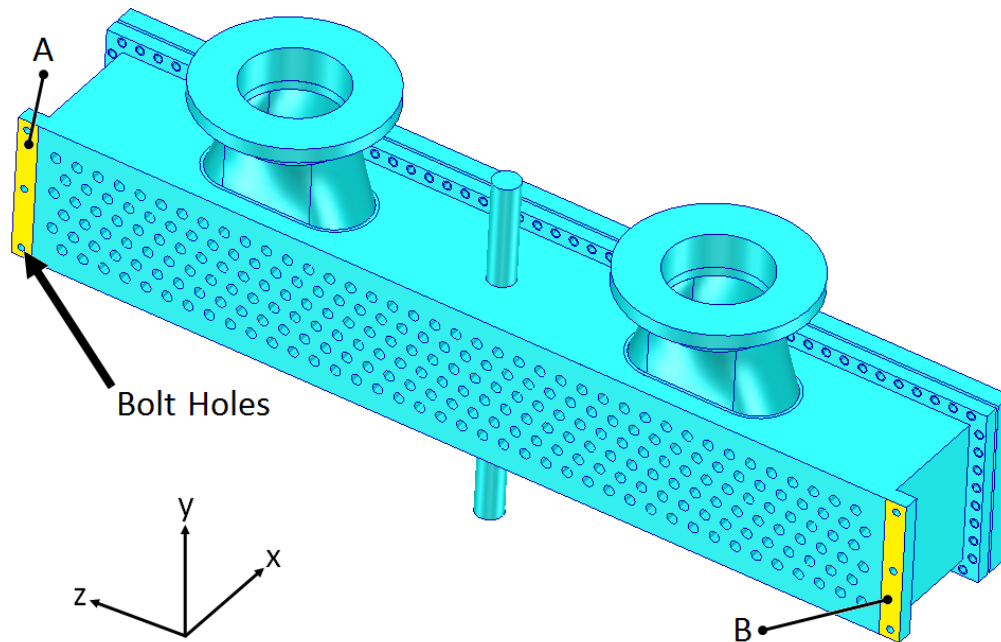
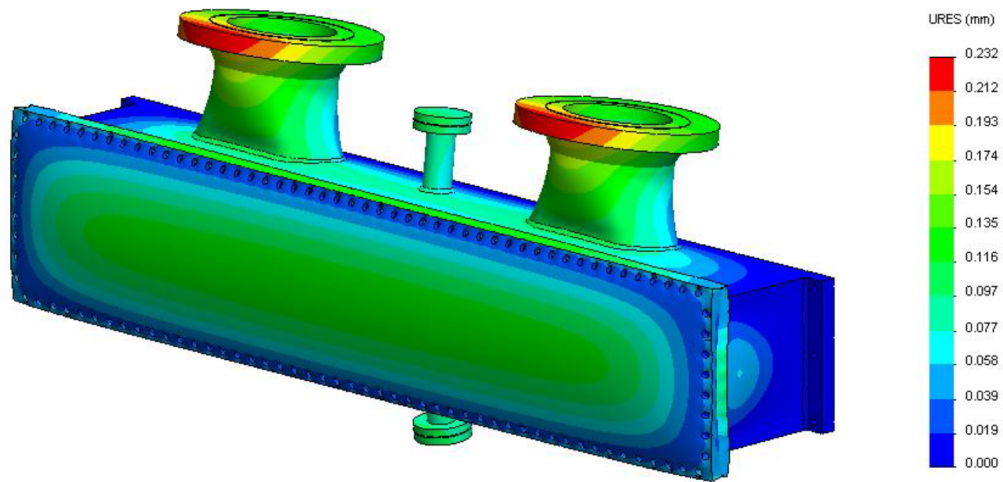


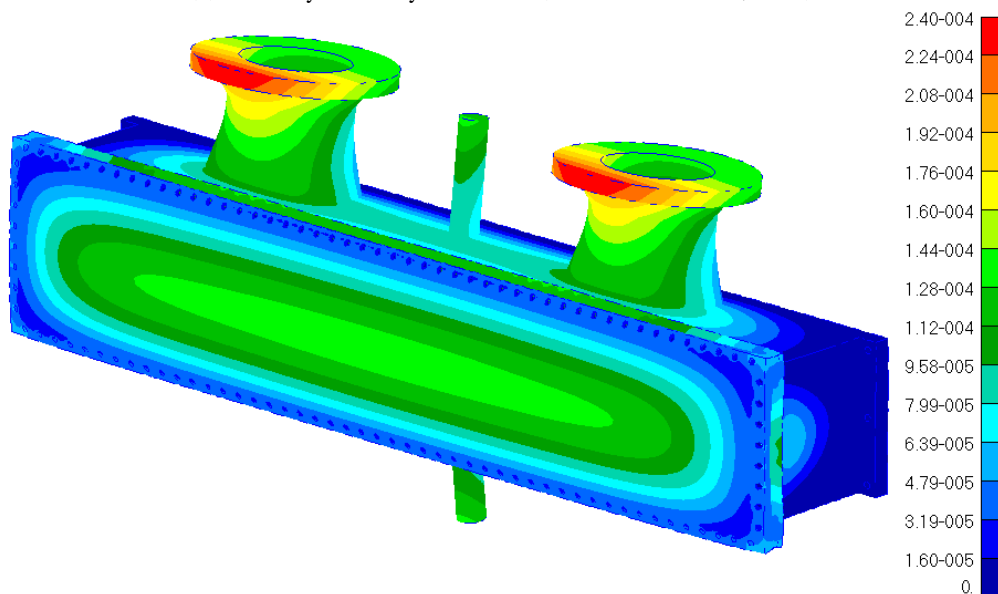
Figure 3.4: Header Box Boundary Conditions

3.1.3 Results And Comparison

This linear model was built and analysed using MSC.Patran 2012 as pre and post processor and MSC.Nastran 2012 as the solver. The model is comprised of 701 597 second order tetrahedral elements. A Young's modulus of 190.5 GPa was used for all header box components, including the gasket, as in the industrial report with which the result were compared. Using these material properties for the gasket was seen as an acceptable simplification because in reality the gasket exhibits highly non-linear structural behaviour. Thus if any other material properties were used to model its structure in this linear analysis, the results would not necessarily be more accurate. A sample of the results obtained are compared with those of the industry report compiled by Axis Mechanical Design in figures 3.5 and 3.6.



(a) Industry FE Analysis Results (F.H. Kraamwinkel, 2013)

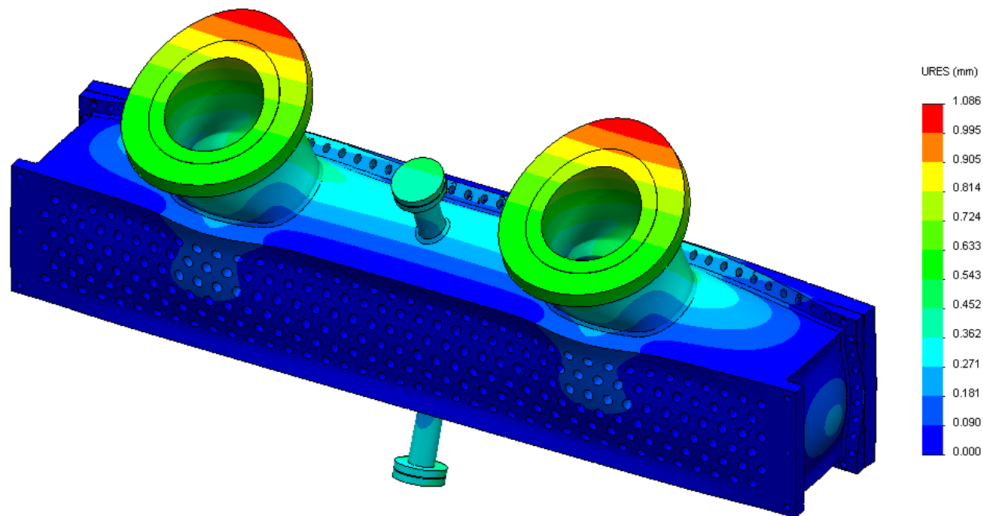


(b) Study FE Analysis Results (m)

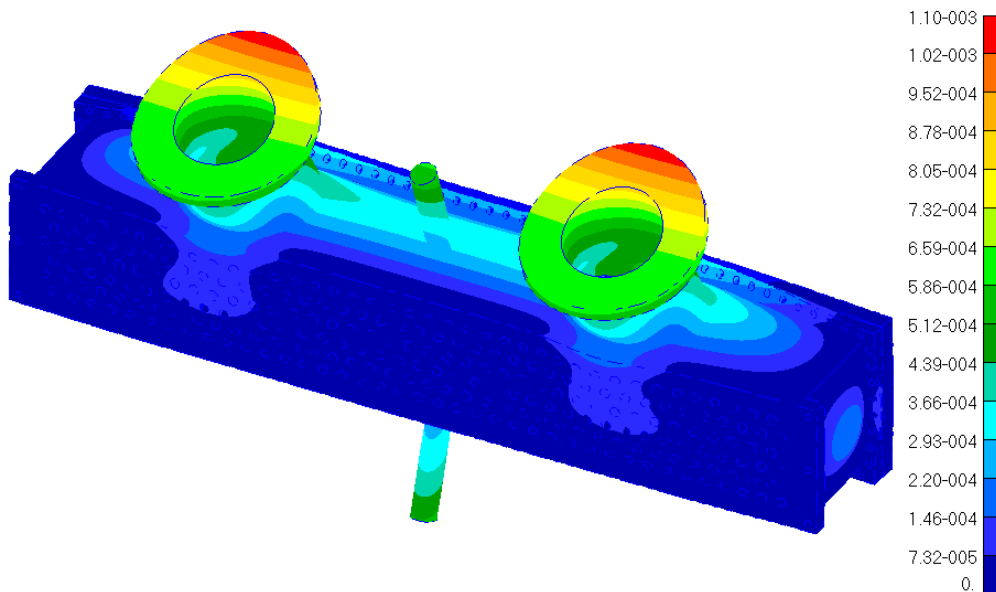
Figure 3.5: Displacement Due To Bolt Loading

Figure 3.5 shows the displacement contour plot for the load case when only bolt loads are applied. In the figure it can be seen that the contour patterns for both sets of results match. In addition, the numerical maximum displacement results of the study's model differ by only 3.3% from those of the industry model.

Figure 3.6 shows the displacement contour plot for the load case where only the loads related to the internal pressure of the box are applied. This includes the nozzle and tubesheet loading and thus comprises the remainder of the loads which were not applied in the bolt loading case. Once again, the contour lines have the same pattern and the numerical maximum results match within 1.3%.



(a) Industry FE Analysis Results (E.H. Kraamwinkel, 2013)



(b) Study FE Analysis Results (m)

Figure 3.6: Displacement Due To Pressure Loading

In order to benchmark this study's model, only the two load cases above need to be compared. This is because any subsequent results needed from the model will be comprised of a linear combination of the results of these two load cases, as bolt and internal pressure are the only load inputs that can be independently modified.

On account of these results, the overall modelling techniques and assumptions are shown to be in line with industry standards, and will therefore be used as the basis for any further FE work in this study.

3.2 3D Linear Model

In the model used for benchmarking, inlet nozzles and individual tubesheet holes were both included. This was done so that an equivalent model could be compared to the FE report available. These features do however not form part of the scope of this study, as they do not form part of the primary concerns with the methodology currently being used for the design of cover type header boxes. Current practice concerning these components is to validate the design of the nozzles and their interface with the header box using a 3D FE analysis and to account for the holes in the tubesheet by including a ligament efficiency, as prescribed by ASME, into the relevant calculations regarding the tubesheet. These components will therefore not be included in all of the subsequent models.

Once these features are removed, the header box becomes symmetric along its length and breadth, as shown in figure 3.7. It is therefore only necessary to model a quarter of the header box, which greatly reduces computation time.

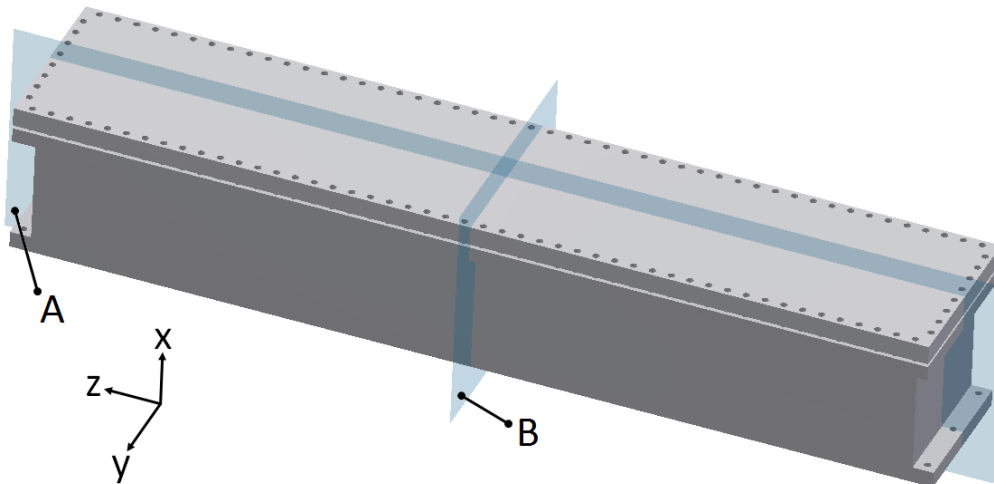


Figure 3.7: Header Box Planes of Symmetry

In order to set up a quarter model of the header box, new boundary conditions need to be applied to simulate the behaviour of the portion of the header box that is not modelled. According to Cook *et al.* (2002), the symmetry boundary conditions that need to be applied are that the displacement perpendicular to any plane of symmetry must be zero. The boundary conditions as applied to this header box model are given in table A.1.

Table 3.1: Symmetric Boundary Conditions

Region	U_x	U_y	U_z
A	Free	Constrained	Free
B	Free	Free	Constrained

Using the design from the same sample case as before, a simulation was run on a header box using the design loads, in order to see how the header box would behave under these conditions. The internal pressure in this case was 2.5 MPa and the load per bolt was 32838 N. The resulting Von Mises stresses are shown in figures 3.8 and 3.9 followed by deflection plot in figure 3.10

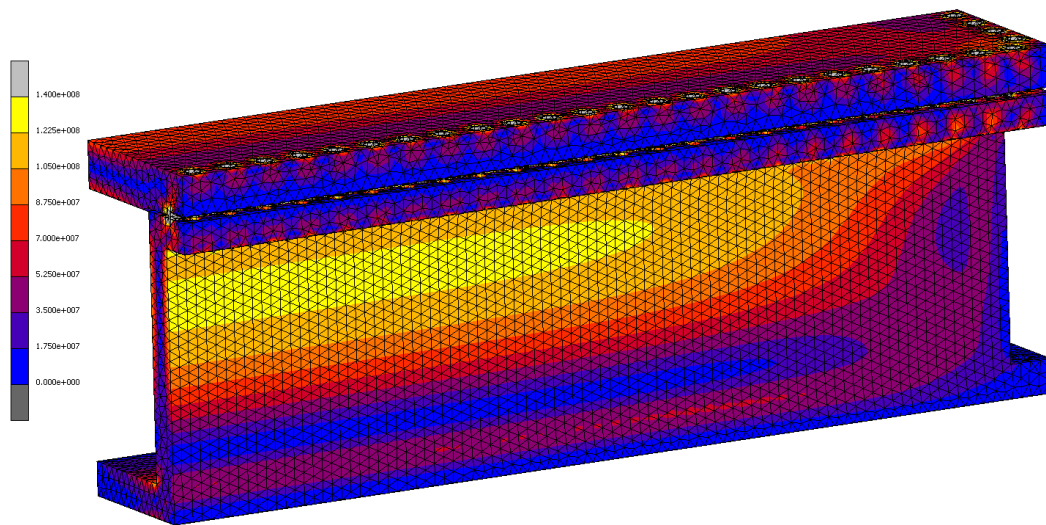


Figure 3.8: Header Box Quarter Model Stress Plot (0-140 MPa)

The results show large contour patterns indicating high stress regions on all of the sides of the header box. When following these patterns along the length of the header box, from the end plate towards the centre, the stress values steadily increase to a maximum at the centre. This can be logically explained by the fact that the end plate of the header box acts as a supporting rib to the cover plate, side plate and tubesheet. Around the area closest to the end plate, the structure is thus strengthened and the three other plates carry less load. Moving away from the end plate, the resulting effect of the support reduces, leading to larger deflections and higher stresses.

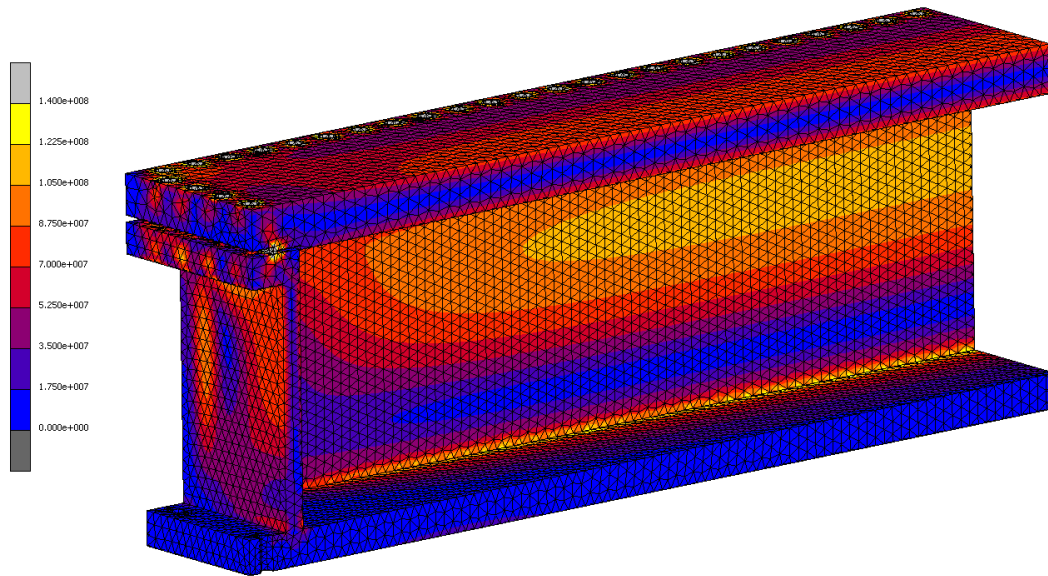


Figure 3.9: Header Box Quarter Model Stress Plot (0-140 MPa)

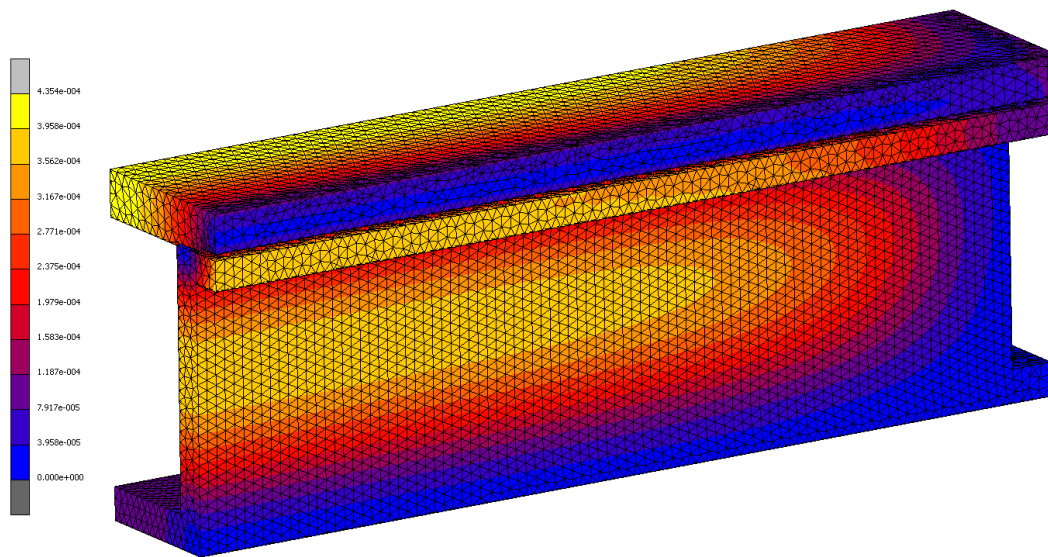


Figure 3.10: Header Box Quarter Model Displacement Plot (0-0.435 mm)

This would suggest that the weakest area of the header box will be half way between the end plates, where the effect of their support is the least. This assumption however only takes into account the general structural behaviour of the header box and does not account for the possibility that a higher stress concentration may form closer to the end plate itself because of structural effects in and around the area where the end plate is joined to the rest of the box.

The only way to know for certain where the header box is weakest is to construct a non-linear FE model which allows the user to track the progress of plastic

deformation in the header box. When tracking plastic deformation, it is possible to differentiate between two possible cases that may occur at points where a high stress concentration is found.

In the first case, the material near the point which is experiencing the high stresses starts to deform plastically. As this happens, the stresses around that point are redistributed and in the process the stress values reduce to a level below the yield strength of the material. The plastic deformation is therefore halted and there is no plastic collapse of the structure.

In the second case, the same process takes place, whereby a point under high stress starts to plastically deform. This time however, the stresses redistribute, but still remain at levels above the material yield strength, or are redistributed in such a manner that new stress concentration points are formed where the stresses are also above the material yield strength. This leads to further plastic deformation in the structure and in turn starts a cascade effect, which may lead to the eventual plastic collapse of the structure. The point where the largest degree of this structural behaviour is observed is likely to be the point where the structure will fail first.

In the following section, a non-linear model of the header box in question will be analysed, in order to find the point on the header box where failure will occur first.

3.3 3D Non-linear Model

The key difference between linear and non-linear FE models that is important for this study is that the non-linear models takes into account material weakening and plastic deformation. A non-linear model works by breaking up the load applied to a model and applying it incrementally. After each increment a new stiffness matrix is set up for the structure which accounts for the weakening of the structure in areas where the yield stress has been exceeded in previous increments.

3.3.1 Material Properties

In order to accurately predict plastic deformation and material weakening, true stress-strain material properties need to be included in the model. Annex 3-D of ASME Section VIII Division 2 (ASME, 2011) provides the necessary equations to set up the relevant material model. The stress-strain behaviour predicted by this material model for the header box's material is shown in figure 3.11. The equations used for these calculations are given in Appendix B.

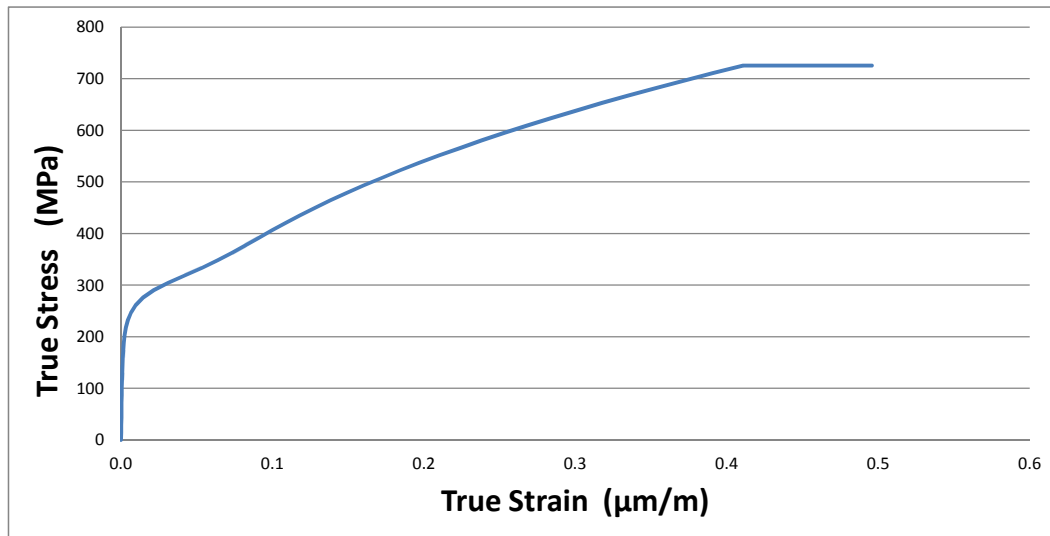


Figure 3.11: True Stress Strain Curve of Header Box Material

3.3.2 Tubesheet Holes

Even though the project scope does not include considering the structural behaviour of individual holes in the tube sheet, these holes were still included in the non-linear model. This was done to check whether any critical secondary stress concentrations would originate due to the proximity between the tube holes and the end and side plate.

3.3.3 Results

The non-linear model was built and analysed using MSC.Mentat 2013 as pre and post processor and MSC.Marc 2013 as the solver. The model was constructed with 168 529 second order tetrahedral elements. The results of this analysis are shown in figures 3.12 and 3.13. These plots show the plastic strain pattern of the header box. In order to see this pattern, loading 6 times larger than the design loads were applied to the header box, in order to ensure that a significant level of plastic deformation was reached. Blue (dark colours) represents the area least affected by plastic deformation leading through to yellow (light colours) which indicates the area most affected by plastic deformation.

Similar to the results in section 3.2, these results also suggest that the critical point on the header box is at the centre, as the highest level of plastic deformation is found here. This behaviour is seen on both the side plate and tubesheet. The only exception to this structural behaviour is an area showing high plastic deformation far from the centre, marked A, in figure 3.14.

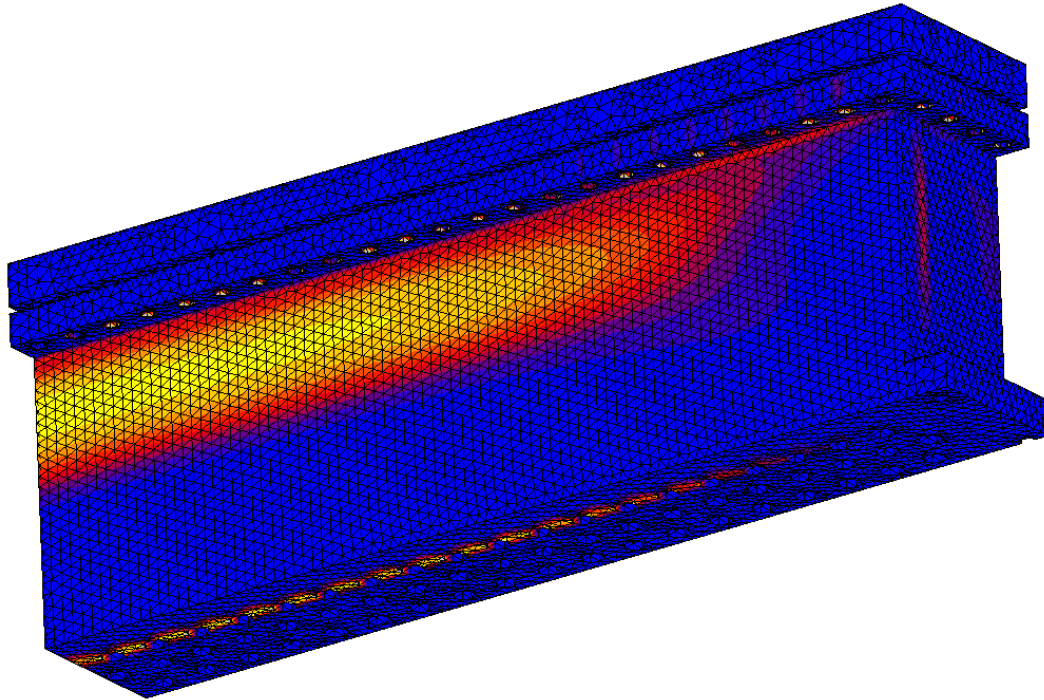


Figure 3.12: Plastic Strain Pattern of Header Box

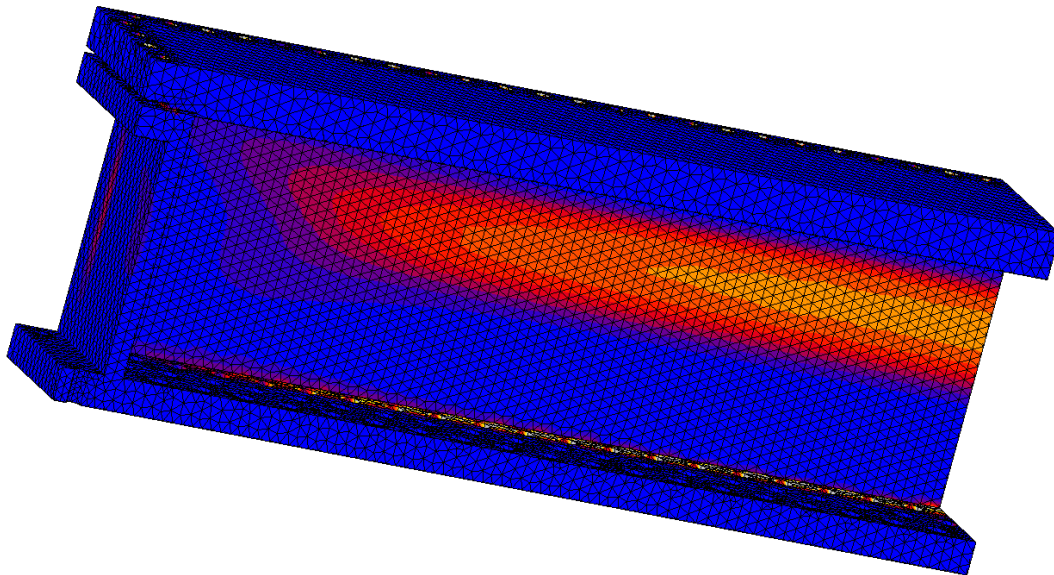


Figure 3.13: Plastic Strain Pattern of Header Box

In order to determine whether the structural behaviour in this area could be more critical to the header box's design than the region at the centre, a comparison was done, tracking the progress of plastic strain, both at the centre of the header box and at the most critical point in region *A*, over a range of load increments applied during the non-linear analysis. Figure 3.15 shows the set of side

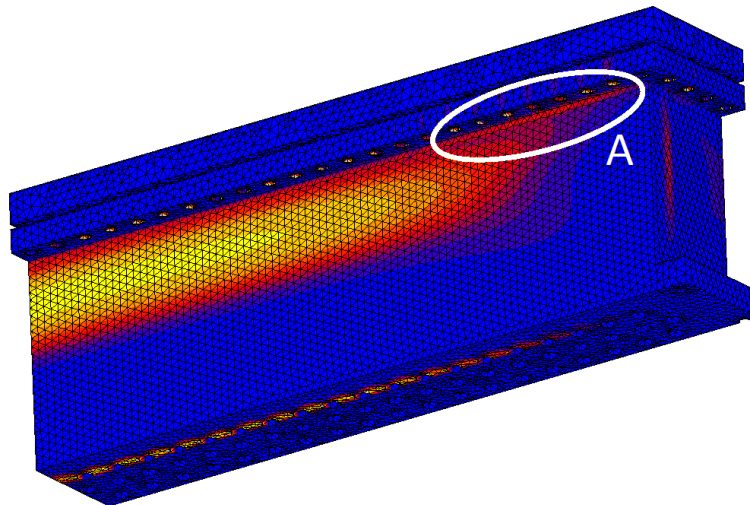


Figure 3.14: Plastic Strain Pattern of Header Box

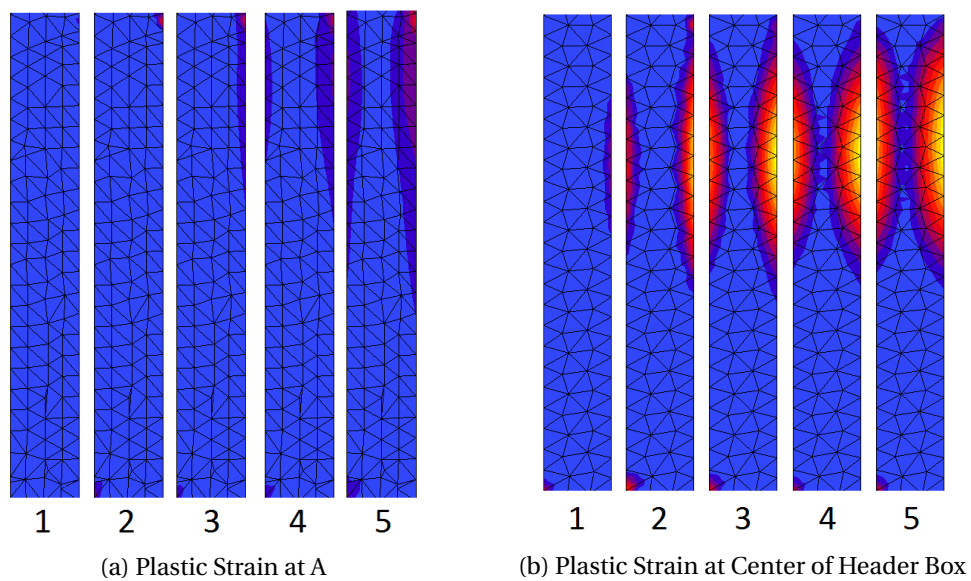


Figure 3.15: Comparison of Plastic Strain for Sequential Load Increments

by side comparisons of the plastic strain in the side plate for both these areas, for sequential load increments.

From this comparison, the centre of the header box is confirmed as the most critical design area, as penetration of plastic deformation takes place far sooner there than in region A.

3.4 Discussion

From these results, it can be deduced that if a header box was infinitely long, the strengthening effect of the end plates would be negligible at the centre of the header box. The resulting stress from a header box model where the end plate structure is ignored will then also necessarily yield a conservative prediction of the stresses in the side plate, cover plate and tubesheet. Furthermore, because a header box without an endplate is essentially a prism, as seen in figure 3.16, it is safe to assume that a full 3D model of a header box can be substituted with a 2D model of the header box's cross-section for the purpose of ensuring the header box's structural integrity.

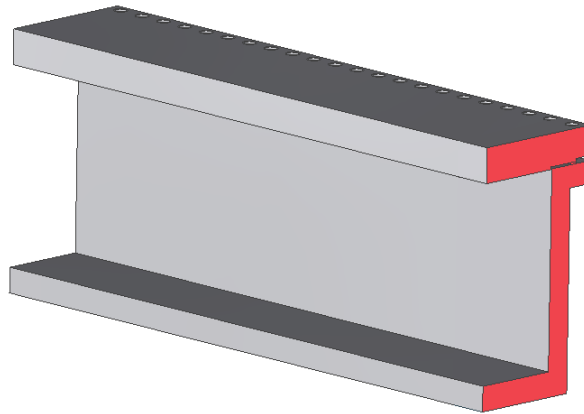


Figure 3.16: Header Box Without End Plate

3.5 2D Model

The main purpose of analysing the header box structure using FE methods was to evaluate the results of the in-house design method used by this study's industrial partner. For this study, only the hand calculation pertaining to the side plate and tubesheet need to be validated, as design of the remaining parts of the header are already covered to a sufficient extent in the ASME and other accepted design code. For this purpose, the 2D FE model provides the perfect solution. Even though the 2D equivalent model of the header box is far more simple than the 3D model, it still provides all the results necessary for analysing the side plate and tubesheet at their critical loading conditions.

At the same time, using the 2D model greatly reduces the computational time needed, from multiple hours for a 3D model to less than a minute for a 2D model.

3.5.1 Boundary Conditions

The 2D model consists of half the cross-sectional profile of the header box, meshed using plain strain elements. The boundary conditions applied to the model are shown in figure 3.17.

A is the boundary condition that enforces the effect of symmetry in the model. All of the nodes along the line of symmetry are constrained from moving in the *y* direction. *B* is the equivalent pressure load applied to the inside of the header box and *C* is the equivalent bolt loads that are applied to the exterior of the header box. Because the bolt geometry is not defined in the 2D model, the bolt loads are applied as a distributed edge load over the portions of the cover plate and flange where the bolt holes would have been situated. Leaving out the bolt geometry was considered an acceptable simplification as the bolt holes are situated far enough away from any point where results will be extracted. The positions where the stress results will be extracted will be discussed in the next section. Finally, *D* is where the model was constrained from moving in the *x* direction at a single node, to prevent a rigid body motion of the FE model.

3.5.2 Results Processing

3.5.2.1 Stress Classification

The guidelines for analysing the results of the FE model are given in ASME Section VIII Division 2 Part 5. The guidelines call for the linearisation of stress results at specific critical positions throughout the structure in order for the bending and membrane stresses to be calculated at these point. The positions where this is done are called stress classification lines (SCL). For the structure in question, figure 3.18 shows where these SCL need to be positioned, as interpreted from guidelines given in ASME Section VIII Division 2 Part 5.

*A*₁, *A*₂ and *C* are positioned at the toe of the welds joining the tubesheet, side plate and flange. The results at these points will check that the header box joints are strong enough. *D* is placed at the center of the tubesheet and *B* is placed at the point along the side plate that experiences the highest combination of membrane and bending stresses. These SCLs check that the tubesheet and side plate will be strong enough.

The method used for performing stress linearisation is illustrated in figure 3.19. The figure shows how the stresses in the local *y* direction, which is perpendicular to the SCL, need to be linearised in order for the membrane and bending stresses to be calculated. The "Peak" stress component in the picture is not relevant in the context of this project as it is primarily used for fatigue failure calculations.

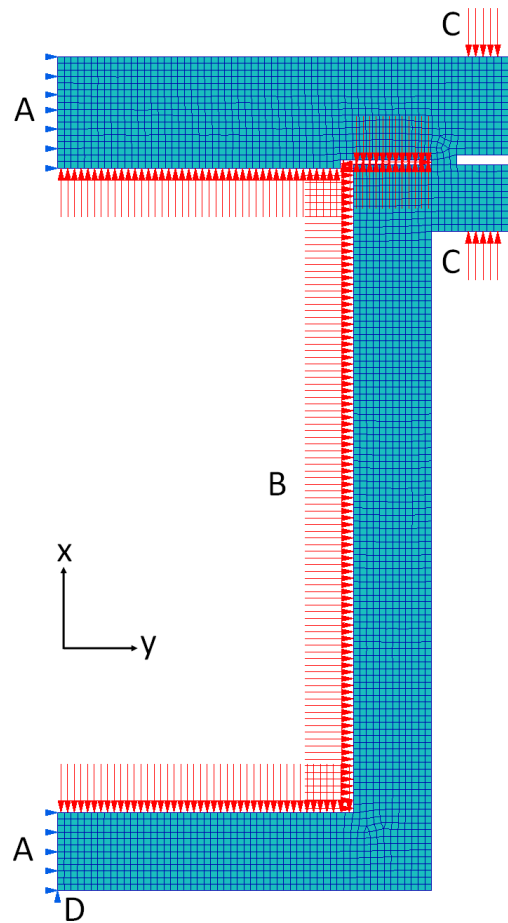


Figure 3.17: 2D Model Boundary Conditions

The formulae used to numerically calculate the components of the membrane and bending stresses are given by equation 3.5.1 and 3.5.2 respectively. In these equations, σ_{ij} represents the component stress values at the nodes along the SCL and t represents the thickness of the structure along the local x direction. Once all the components of the membrane and bending stresses are calculated, a von Mises calculation is used to calculate the final representative membrane stress and bending stress. It must be noted here that for calculating the bending stress, all stress component running parallel to the SCL must not be considered.

$$\sigma_{ij,m} = \frac{1}{t} \int_0^t \sigma_{ij} dx \quad (3.5.1)$$

$$\sigma_{ij,b} = \frac{6}{t^2} \int_0^t \sigma_{ij} \left(\frac{t}{2} - x \right) dx \quad (3.5.2)$$

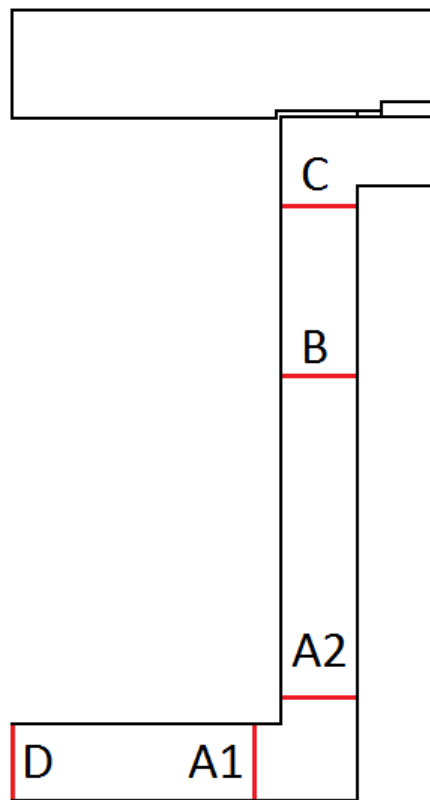


Figure 3.18: SCL Positions

3.5.2.2 Acceptance Criteria

ASME Section VIII Division 2 Part 5 also provides failure criteria against which the stress values extracted from a structure, need to be compared. The criteria that need to be satisfied are:

$$\sigma_1 + \sigma_2 + \sigma_3 \leq 4S \quad (3.5.3)$$

where S is the allowable header box material stress and σ_1 , σ_2 and σ_3 are the principle stresses in the structure.

$$P_m \leq S \quad (3.5.4)$$

$$P_L \leq 1.5S \quad (3.5.5)$$

$$P_L + P_b \leq 1.5S \quad (3.5.6)$$

$$P_L + P_b + Q \leq 3S \quad (3.5.7)$$

where P_m is the general primary membrane equivalent stress, P_L is the local primary membrane equivalent stress, P_b is the primary bending equivalent stress and Q is the secondary equivalent stress.

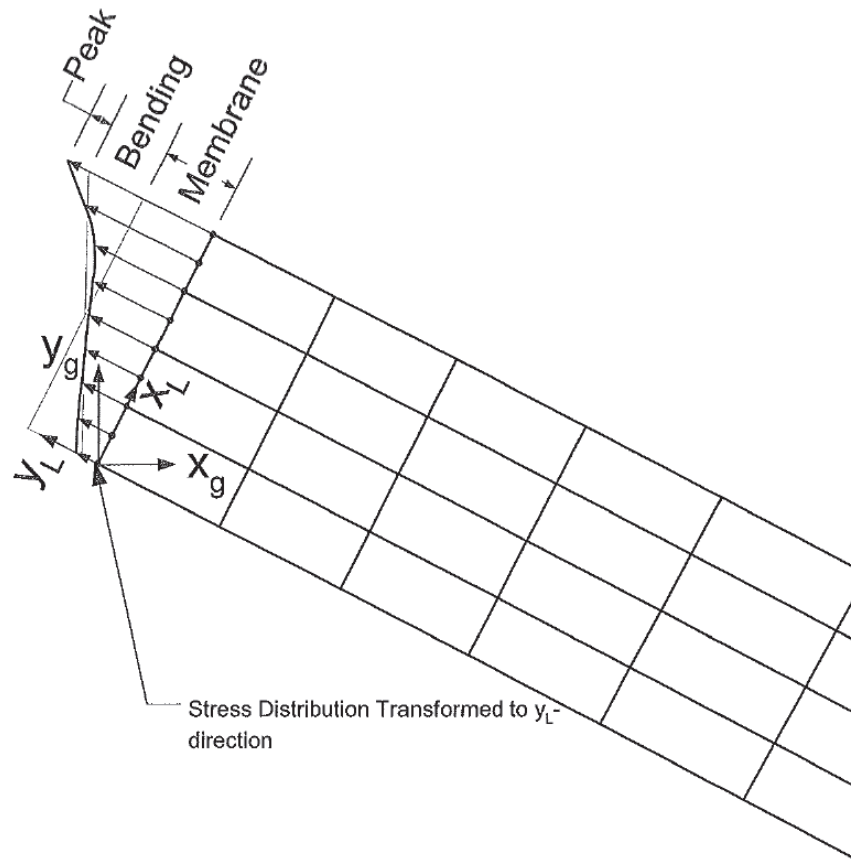


Figure 3.19: Stress Linearisation Diagram (ASME, 2011)

Table 3.2 presents a modified extract from table 5.6 in Part 5 of ASME VIII Division 2, which shows how to classify the stresses in the header box model in order to determine which values need to be applied to the criteria given above.

Table 3.2: Stress Classification Guide

Location	Type of Stress	Classification
Center Region [B,D]	Membrane	P_m
	Bending	P_b
Junction to shell [A1,A2,C]	Membrane	P_L
	Bending	$Q^{[1]}$

[1] If a bending moment at the edge is required to maintain the bending stress in the center region within acceptable limits, the edge bending is classified as P_b ; otherwise, it is classified as Q

The exception in this table practically means that if the tubesheet or the side plate is not strong enough to support the loading placed on it, without any support from the joints it is connected to, the bending stress at those joint will be classified as P_b instead of Q .

The method for showing whether the tubesheet or side plate meets this criteria, is to simplify the relevant plate to a simply supported beam, as done by the hand calculations in chapter 2. Using beam theory, the membrane and bending stresses can then be calculated at the centre of that plate. If these values satisfy the necessary failure criteria, the bending stress classification at the joints stay as they are, but if they do not, exception [1] needs to be applied.

Using the guidelines from table 3.2, the failure criteria given above can be interpreted to practically mean the following:

At points B and D , which are located in the central regions of the side plate and tubesheet respectively

$$\sigma_m \leq S \quad (3.5.8)$$

$$\sigma_m + \sigma_b \leq 1.5S \quad (3.5.9)$$

At points $A1$, $A2$ and C , which are at the joints between the tubesheet, side plate and flange

$$\sigma_m \leq 1.5S \quad (3.5.10)$$

$$\sigma_m + \sigma_b \leq 3S \quad (3.5.11)$$

However, if exception [1] is applicable

$$\sigma_m + \sigma_b \leq 1.5S \quad (3.5.12)$$

The results produced by this model are discussed in the next chapter.

Chapter 4

Results and Comparison

In this chapter, results will be presented for four dissimilar header designs that were analysed using the 2D model presented in chapter 3. These results are then compared to the results predicted by the hand calculations from chapter 2, followed by a critical discussion.

4.1 2D Model Results

Figure 4.1 shows the Von Mises stress plots for the four header box design analyses in this chapter, which include the design used for testing in chapter 3. The header box designs used were analysed again using a linear solver in MSC.Marc. The models were constructed using an average of roughly 2000 Q8 plain strain elements. The geometric details of these designs can all be found in Appendix A.

The numerical results from these models, calculated at the stress extraction points according to equations 3.5.1 and 3.5.1 in chapter 3, are given in table 4.1. The critical failure criteria applicable at each point and the percentage by which the structure exceeds the necessary design is also given. This percentage was calculated as shown in equation 4.1.1, using the relevant stress values for the critical criteria.

$$\% \text{ over design} = \frac{|\sigma_{allowable} - \sigma_{recorded}|}{\sigma_{recorded}} \quad (4.1.1)$$

In the tables, D' is the results at point D before they have been modified to take into account the fact that the tubesheet is a perforated plate which has a reduced load carrying capacity. The values at D were calculated by dividing the original results by a perforated plate ligament efficiency factor, which was calculated using equation 4.1.2,

$$e = \frac{P_t - d_1}{P_t} \quad (4.1.2)$$

where P_t is the pitch and d_1 is the diameter of the holes in the tubesheet.

The high stresses seen around the gasket are not considered. As stated before, the gasket exhibits highly non-linear structural behaviour. Thus in these linear analyses the stresses predicted for the gasket and its immediate surroundings are not reliable. This is however not a problem as this study is not concerned with how well the header box seals at the gasket and therefore does not require accurate stress values in this area.

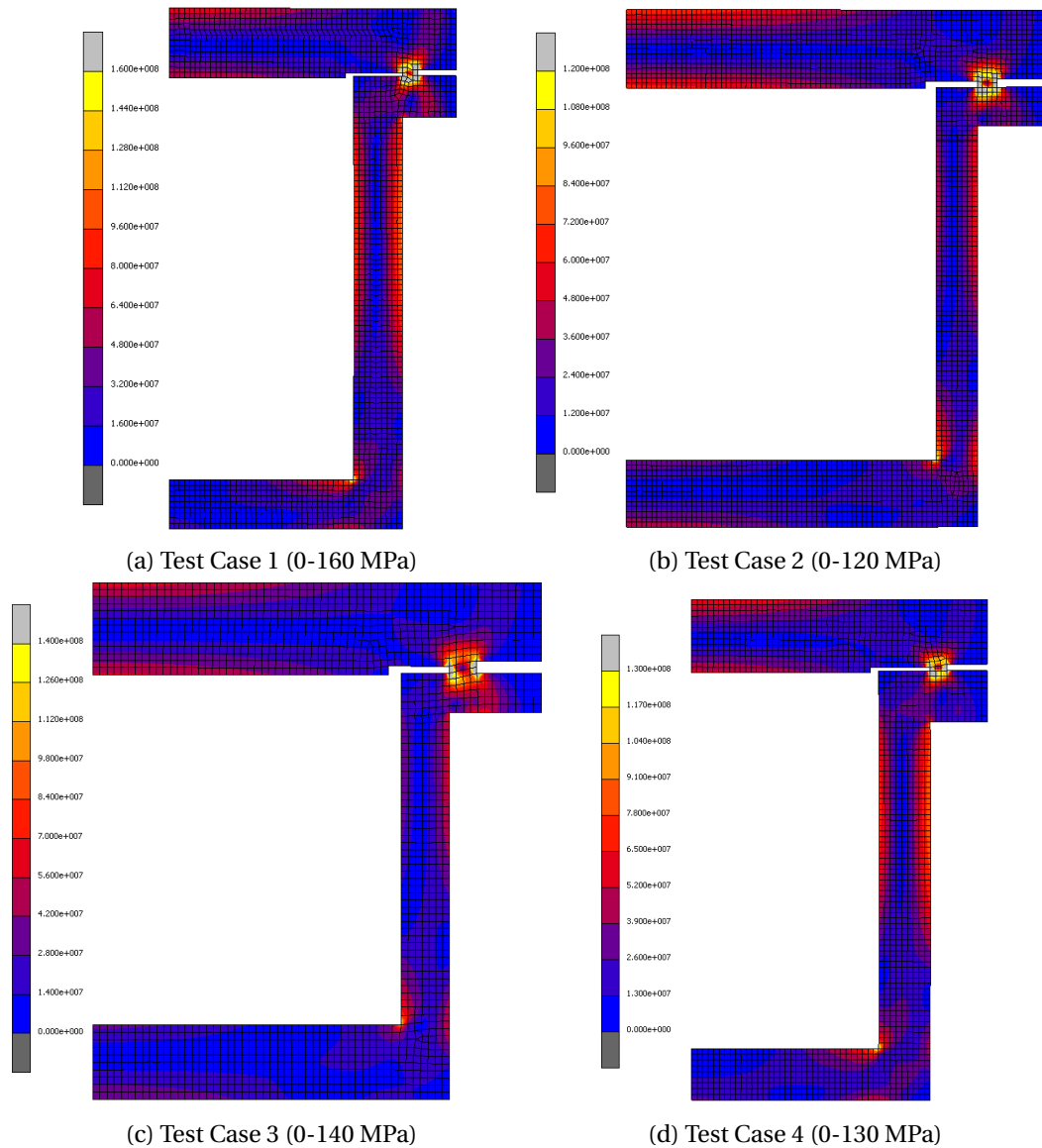


Figure 4.1: Von Mises Stress Plots for 2D Finite Element Test Cases

Table 4.1: 2D Finite Element Model Results

Position	σ_m (MPa)	σ_b (MPa)	Critical Failure Criteria	% Over Design
Test Case 1				
A1	18.4	87.3	$\sigma_m + \sigma_b \leq 3S$	292
A2	22.1	71.1	$\sigma_m + \sigma_b \leq 3S$	344
B	12.0	123.1	$\sigma_m + \sigma_b \leq 1.5S$	53
C	11.7	95.1	$\sigma_m + \sigma_b \leq 3S$	288
D	26.7	15.9	$\sigma_m + \sigma_b \leq 1.5S$	387
D'	13.9	8.3	$\sigma_m + \sigma_b \leq 1.5S$	832
Test Case 2				
A1	11.5	34.5	$\sigma_m + \sigma_b \leq 1.5S$	800
A2	16.3	83.1	$\sigma_m + \sigma_b \leq 3S$	316
B	10.7	62.6	$\sigma_m + \sigma_b \leq 1.5S$	182
C	10.7	53.9	$\sigma_m + \sigma_b \leq 3S$	541
D	10.0	79.9	$\sigma_m + \sigma_b \leq 1.5S$	130
D'	5.7	45.7	$\sigma_m + \sigma_b \leq 1.5S$	303
Test Case 3				
A1	11.2	29.9	$\sigma_m + \sigma_b \leq 3S$	907
A2	16.3	66.4	$\sigma_m + \sigma_b \leq 3S$	401
B	10.7	57.4	$\sigma_m + \sigma_b \leq 1.5S$	204
C	10.5	55.0	$\sigma_m + \sigma_b \leq 3S$	532
D	9.6	70.0	$\sigma_m + \sigma_b \leq 1.5S$	160
D'	5.9	43.1	$\sigma_m + \sigma_b \leq 1.5S$	322
Test Case 4				
A1	17.2	68.4	$\sigma_m + \sigma_b \leq 3S$	384
A2	19.7	57.1	$\sigma_m + \sigma_b \leq 3S$	439
B	9.8	93.4	$\sigma_m + \sigma_b \leq 1.5S$	101
C	10.4	78.0	$\sigma_m + \sigma_b \leq 3S$	368
D	20.9	32.6	$\sigma_m + \sigma_b \leq 1.5S$	287
D'	12.4	19.4	$\sigma_m + \sigma_b \leq 1.5S$	551

4.2 Results Comparison

In this section, the 2D FE results, for the four test cases presented, will be compared to stress values predicted by the hand calculations from chapter 2.

First, the membrane stresses for all the stress extraction points will be compared. The values for this comparison are presented in Table 4.2.

Table 4.2: Membrane Stress Results Comparison

	FE Results	Hand Calculation	% Diff	FE Results	Hand Calculation	% Diff
	Test Case 1			Test Case 2		
A1	18.4	20.1	9.4	11.5	7.1	38.4
A2	22.1	9.5	56.9	16.3	10.3	36.6
B	12.0	9.5	21.0	10.7	10.3	3.7
C	11.7	9.5	18.7	10.7	10.3	3.9
D	26.7	20.1	24.7	10.0	7.1	29.0
	Test Case 3			Test Case 4		
A1	11.2	6.8	39.1	17.2	15.5	10.1
A2	16.3	10.3	37.0	19.7	9.1	53.7
B	10.7	10.3	4.0	9.8	9.1	7.0
C	10.5	10.3	2.3	10.4	9.1	12.4
D	9.6	6.8	29.0	20.9	15.5	25.7

From the results it is seen that the FE analysis and hand calculations only yield similar results for stress extraction points *B* and *C*. The results across the board however, except for one point, show that the hand calculations predict non-conservative membrane stresses.

The reason for the hand calculations predicting lower stresses can be explained by the fact that the hand calculations use an overly simplified method for calculating the membrane stresses in the walls of the header box. The equation used to calculate the membrane stresses simplifies to,

$$S_m = \frac{F}{A} \quad (4.2.1)$$

where A is the cross-sectional area of the wall in question and F is the force acting axially through the wall. In the hand calculations, the value for F is however

calculated based only on the pressure loading and does not take into account the effect that the bolt loading has on the header box. It therefore makes sense that the FE results, which do take the bolt loading into account, yields larger membrane stress values for the structure for all four test cases.

The following part of the comparison will look at the bending stresses in the header box. First points *A1*, *A2* and *C* will be considered. These points represent the joints of the header box. Table 4.3 provides the relevant values for this comparison.

Table 4.3: Bending Stress Results Comparison at *A1*, *A2* and *C*

	FE Results	Hand Calculation	% Diff	FE Results	Hand Calculation	% Diff
	Test Case 1			Test Case 2		
<i>A1</i>	87.3	33.6	28.6	34.5	15.5	55.1
<i>A2</i>	71.1	33.6	12.4	83.1	40.6	51.1
<i>C</i>	95.1	-	-	53.9	-	-
	Test Case 3			Test Case 4		
<i>A1</i>	29.9	12.4	58.5	68.4	46.8	31.6
<i>A2</i>	66.4	23.2	65.1	57.1	46.8	18.0
<i>C</i>	55.0	-	-	78.0	-	-

From these results we see that the FE analyses predicted significantly larger bending stresses at the header box joints than the hand calculations, but also that the hand calculations does not calculate any stress value at the joint between the flange and the side plate. This shows that the simplified beam theory analysis method used in the hand calculations do not have the ability to accurately capture the complex nature of the stresses occurring at the header box joints.

When looking at the bending stress comparison for the centre of the tubesheet (point *D*), as shown in table 4.4, we see the opposite trend. Here the FE analysis results show a far lower bending stress than the hand calculations, for all the test cases. The variation in results can be explained by the fact that the hand calculations attempt to predict the stresses in the tubesheet by adding the results from three different load cases together. These load cases account for the bolt loading, pressure loading and attempt to simulate the 90° angle which is enforced between the tubesheet and side plate. In order to arrive at each of these load cases, simplifications need to be made to the original structure. Very often

such simplifications are conservative in nature. It is thus conceivable that at this point in the structure, the combination of the assumptions have lead to an overly conservative stress prediction.

Table 4.4: Bending Stress Results Comparison at D

Test Case	FE Results	Hand Calculation	% Diff
1	15.9	141.5	364.8
2	79.9	127.6	59.7
3	70.0	152.3	117.6
4	32.6	88.1	148.8

Finally, looking at the bending stress in the side plate (point B), we see that the FE analysis show higher stress than those predicted by the hand calculations, as shown in table 4.5. For this comparison, it must be noted that the two different methods are also predicting different positions for the maximum bending stress. As shown in figure 4.2 A, the hand calculations reduce the side plate to a simply supported beam with symmetric bending. Thus, it predicts that the maximum stress will occur at the centre of the plate. In reality however, the boundary conditions on the side plate are much more similar to B in figure 4.2, which results in the position of the maximum stress moving up higher along the side plate as the bolt load increases. Unlike the hand calculations, the FE software is able to more accurately capture the complexity of the side plate's boundary conditions, thus giving a better indication of what the maximum bending stress will be and where it will be found.

Table 4.5: Bending Stress Results Comparison at B

Test Case	FE Results	Hand Calculation	% Diff
1	123.1	97.5	20.8
2	62.6	45.3	27.6
3	57.4	44.6	22.3
4	93.4	56.0	40.0

4.3 Discussion

When considering the results in this chapter, an important question arises: If the current design methods being used appear to be so non-conservative, why

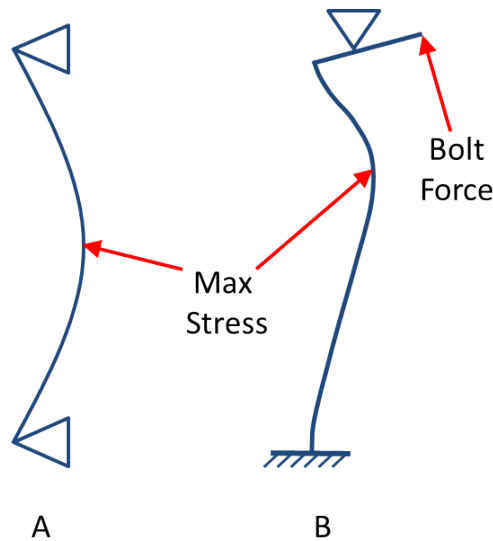


Figure 4.2: Side Plate Boundary Conditions

are their resulting header box designs so over conservative. To answer this question, the focus must first be taken away from the actual design method's calculations and be shifted to look at how a designer uses the results predicted by these methods and what the influence of external factors are on the final design of a header box.

First, consider some of the external factors that influence the design of a header box, over and above the results from the design calculations. The metal plate used to construct header boxes is only available in set size intervals. Therefore, any calculated optimal design will automatically be rounded up to fit these values.

A second external factor is that a manufacturer will sometimes elect to increase the thickness of the material used to construct certain parts of a header box, in order for them to match the thickness of one or more of the other sides of the box. These decisions are usually motivated by logistical considerations, such as it being cheaper or less complicated to order a larger quantity of a single size of sheet metal than to order multiple metal plates having different thicknesses. Another reason for this is that a manufacturer may already have stock of a certain size of metal plate, which is thicker than what is required, and choose to rather start construction earlier with this material in hand than to wait for a new order.

A final external factor, which is motivated by a manufacturing requirement, is that a header box's tubesheet thickness has to equal or exceed the thickness of the side plates. According to manufacturers, if the tubesheet is thicker than the side plate, the resulting joint must be welded from the side plate's side of the joint

and vice versa, as illustrated in figure 4.3. If the joint is however welded from the tubesheet's side, the heat affected zone of the metal, where the material is then hardened, overlaps with where the tubesheet holes need to be drilled. Drilling these holes therefore becomes much more expensive as the cutters become blunt sooner and break more often.

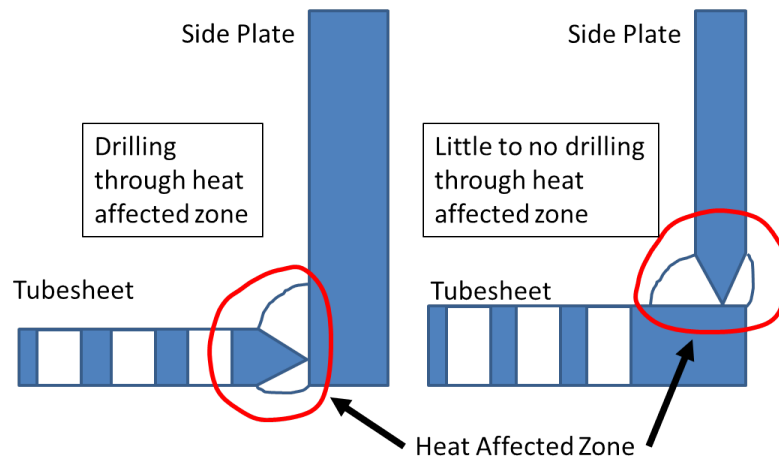


Figure 4.3: Welding Detail

In addition to these factors, there is also a human factor that comes into play, which tends to make header box designs more conservative. As a result of the concern linked to the validity of the hand calculation being used, designers tend to err on the side of caution and rather increase material sizes if they are at all uncertain, in a bid to ensure that their design will definitely be safe. In the process of reviewing header box designs based on current practice hand calculations, this trend was encountered often. In these cases, an extra material thickness increment of 5mm was found added onto the optimal design, as determined by the hand calculations, even after all of the external influencing factors mentioned above had been taken into account. In the end, it is the compounded effect of all these factors that finally lead to a header box being significantly over designed.

Chapter 5

Proposed Solution

The primary objective of this project was to implement design phase changes to the way header boxes are designed, in order to increase the credibility and accuracy of the process. In order to achieve this goal it was decided to incorporate the results from a 2D FE analysis into the header box design pack, along with the hand calculations from chapter 2. This would serve to analyse the header box structure in more detail and validate the hand calculations for each design case, thereby giving more credibility to the design.

5.1 Software Structure And Components

In order to practically implement this plan, a new software package was developed that would automatically set up and analyse a 2D FE model of a cover type header box, based on a fixed set of parameters. Included in this package is also an optimiser that seeks to minimise the material used to construct the header box, while taking into account the material and manufacturing factors that influence a headed box's design.

The principle reasons for choosing to develop new software rather than working with products available on the market were that:

1. New software can be coded on an open source platform, thus avoiding costly license fees
2. New software can be tailored to perform exactly the task needed without any unnecessary features that complicate its use.

The program developed consists of four parts, coded in a collection of Excel VBA, Python and Octave. Figure 5.1 shows the structure of how these parts interact and what their main functions are.

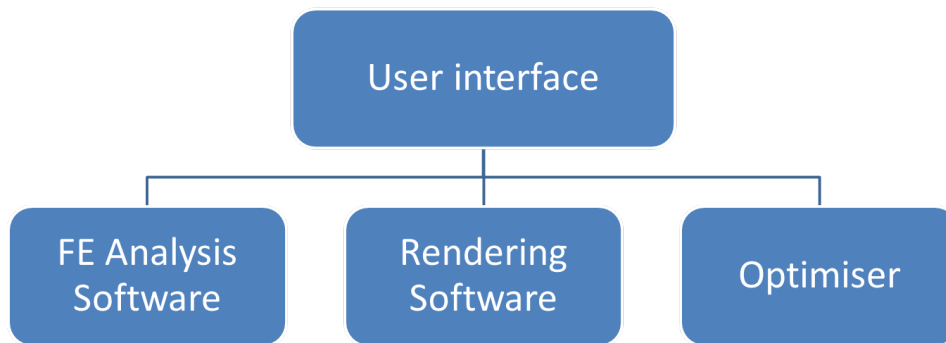


Figure 5.1: Program Structure

5.1.1 User Interface

As part of the design process already in use by this project's industrial partner, all the information pertaining to a new header box's design is deposited into an Microsoft Excel document. Motivated by this, it was decided to base the user interface portion of the new software in this Excel document in order to integrate its functionality as seamlessly as possible into the design process already in use.

An additional reason for choosing Excel rather than another platform for the user interface was that most people are already familiar with Excel. Thus most new users would immediately be able to operate the new software without the need for additional training. The final benefit of using Excel is that it already features a large collection of build in visual tools with which to create an easy to operate users environment, thus eliminating the need to create such an environment from in a new software platform.

The user interface operates as a platform where the user inputs a set of parameters describing the geometry and loading of a header box. From here the user can set certain preferences, such as mesh size and design factors, before performing a FE analysis on the header box. Once the analysis is complete, the results can be imported back to this interface, where they are then automatically processed to determine whether the header box meets the necessary failure criteria as set out in section 3.5.2.2. In addition to running a single analysis, the user can also choose to run an optimization sequence that will run multiple analyses in order to determine the optimal design for the header box being considered. Lastly, the interface allows the user to call for various results to be visually rendered in order to help the user understand the results. The layout of the interface is shown in figure 5.2.

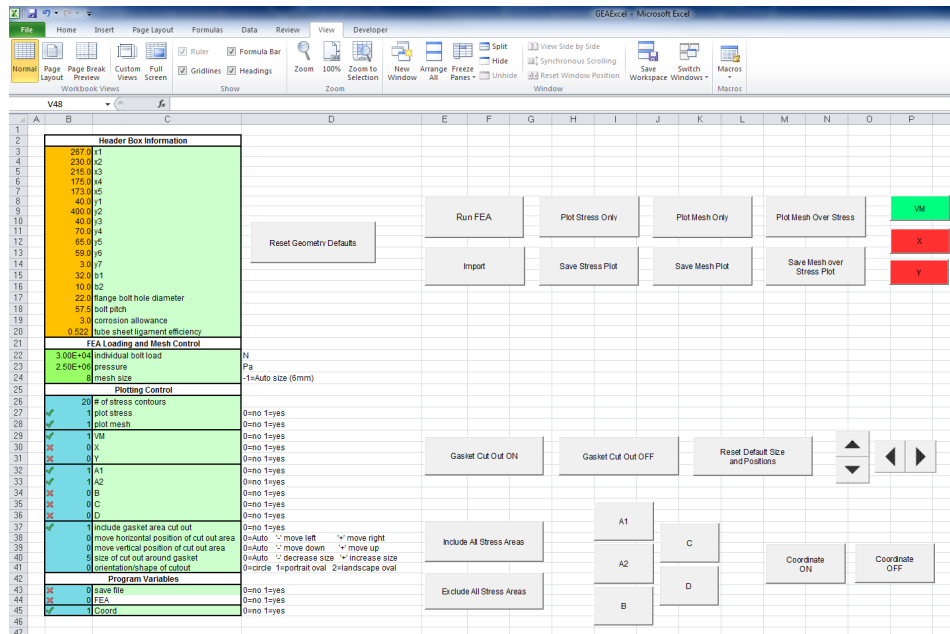


Figure 5.2: Graphical User Interface

5.1.2 FE Analysis

Once all the information about the header box is defined in the graphical user interface, the FE analysis software takes over and automatically constructs a 2D FE model of the header box and performs an analysis on its structure.

The procedure followed by the program is as follows:

1. Mesh the header box structure according to the user's mesh size preference
2. Apply the relevant loads and boundary conditions
3. Set up a system of linear equations describing the structure
4. Solve for the stresses in the header box

5.1.2.1 Element Formulation

In setting up the FE analysis code, it was decided to use an assumed stress element called $5\beta - NT$ in this FE software. The reason for using this element rather than more widely known displacement based elements such as the Q4 or Q8 is that assumed stress elements can analyse a structure to the same degree of accuracy as displacement based element while using fewer nodes and degrees of freedom (Groenwold, 2014). This element therefore increases the computational efficiency of the FE package allowing for analyses to be performed faster.

The coding of the elements was done according to the element formulations given by Di and Ramm (1994). A simplified version of these formulations is provided in appendix C.

5.1.2.2 Boundary conditions

For convenience, the boundary conditions applicable to the 2D model are again described here and shown in figure 5.3. In the figure, *A* is the boundary condition that enforces symmetry in the model. This boundary condition requires that all the nodes along *A* are constrained from moving in the *y* direction.

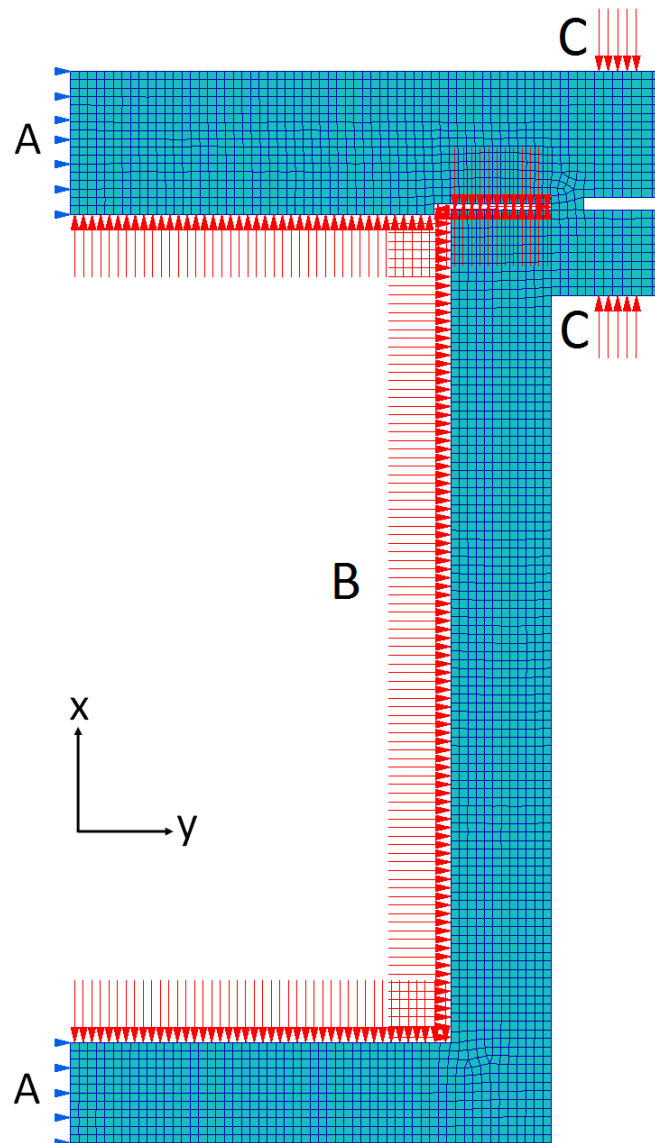


Figure 5.3: Boundary Conditions

B and C represent the equivalent internal pressure and bolt loads that are applied to the model. The size of these loads are calculated using equations 5.1.1 and 5.1.2. Both B and C have the units of force per unit length, and they are calculated on the basis that the model has a thickness equal to one bolt pitch, P_b , along the length of the box.

$$B = PP_b \quad (5.1.1)$$

$$C = \frac{F_b}{N_b} \quad (5.1.2)$$

Here, P is the internal pressure, F_b is the total design bolt load and N_b is the number of bolts in the header box.

5.1.2.3 Stress Extraction and Classification

Finally, after the structure has been set up and analysed, the software extracts the relevant nodal stress values and calculates the bending and membrane stresses that need to be compared to the failure criteria for the structure. For convenience, the positions where the stresses are extracted are shown again in figure 5.5, followed by the relevant failure criteria that needs to be met in table 5.1.

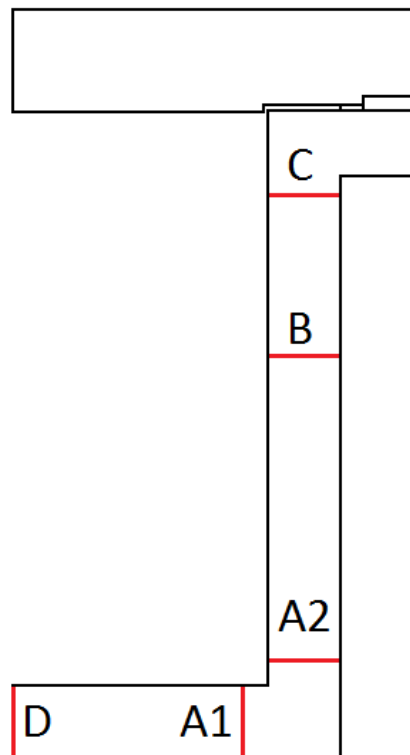


Figure 5.4: Stress Classification Line Positions

Table 5.1: Acceptance Criteria

Points: A1, A2, B, C, D		
$\sigma_1 + \sigma_2 + \sigma_3$	\leq	$4S$
Points: A1, A2, C		
σ_m	\leq	S
$\sigma_m + \sigma_b$	\leq	$1.5S$
Points: B, D		
σ_m	\leq	$1.5S$
$\sigma_m + \sigma_b$	\leq	$3S$
	or	
$\sigma_m + \sigma_b$	\leq	$1.5S^{[1]}$
[1] Only applicable if a bending moment at the edge is required to maintain the bending stress in the center region of the tubesheet or side plate within acceptable limits		

5.1.3 Results Rendering

After the structure has been analysed, the rendering part of the software allows the user to visualise the stress results in the form of a contour plot that shows the stress patterns in the header box cross section. The user can configure these result plots as required, giving him/her the option to decide whether to plot the stresses in the x direction, y direction or the Von Mises stress. Furthermore the user can choose to annotate the plot to show the stress extractions points, coordinate frame reference or the mesh that was used in the analysis. A sample of the possible results output is shown in figure 5.5. Finally, the user has the option to hide the high stress area around the gasket in order to show a clearer stress pattern for the rest of the structure. The advantage of this feature is illustrated in figure 5.6.

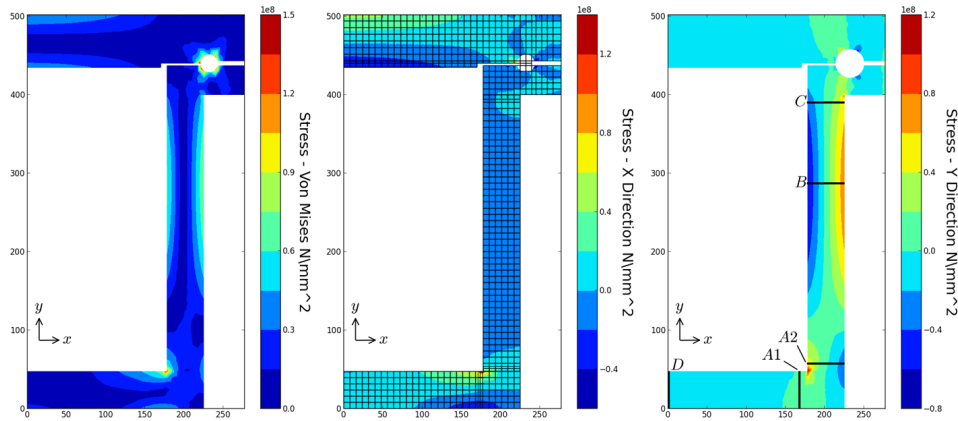


Figure 5.5: Sample Results From New FE Software

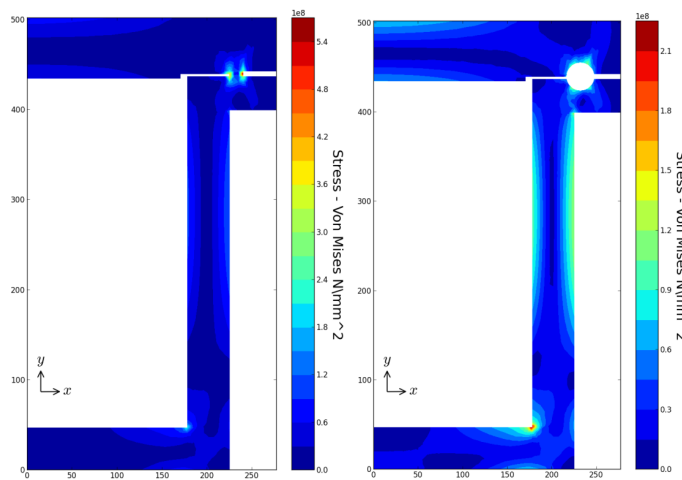


Figure 5.6: Results With and Without Gasket Stresses Hidden

5.1.4 Optimisation

After experimenting with a genetic algorithm optimiser and looking at constrained gradient based optimisation, it was decided to rather use an optimiser that follows a simple search pattern in order to determine the optimum design. The primary reason for this decision was that this technique would require the least amount of function evaluation before reaching the optimum design. This is because the problem at hand only had two design variables and it was only necessary to optimize to the nearest available metal plate thickness. Therefore the pool of possible answers was small enough for the search pattern optimiser to be more effective than the other methods considered.

The objective function of the optimisation problem was to minimize the cross-sectional area of the tubesheet and the side plate, while satisfying all constraints. The primary constraints were that the stress in the header box material was not

allowed to exceed the failure criteria set out in section 5.1.2.3. Additional constraints were that the tubesheet thickness had to be equal or exceed the thickness of the side plates and that only available material sizes could be used. These constraints were added so that the optimiser would account as far as possible for all the external factors that influence the design of a header box, as discussed in 4.3, thus meaning that a predicted optimal design would be suitable for construction as is.

Figure 5.7 shows a flow chart of how the search pattern optimiser works. To start with, a FE analysis is performed using an initial wall thickness supplied by the user. For the first analysis, both the tubesheet and side plate are set to the same wall thickness. The results are then analysed to determine whether any of the constraints are being violated at that wall thickness. If any constraints are violated, the optimiser proceeds to increase the wall thickness in large increments, two material sizes at a time, while successively performing analyses and check the constraints. This is done until all the constraints are no longer violated. Up to this point, the tubesheet and side plate wall thicknesses are kept equal to one another. From here, the optimiser proceeds to perform a limited exhaustive search, using varying wall thickness combinations for the tubesheet and side plate, in order to determine what the optimum design will be. If after the first analysis no constraints were violated, this process is simply followed in reverse by first decreasing the wall thicknesses incrementally before performing a final search. The results yielded by the optimiser will be discussed in chapter 6.

5.2 Program Validation

5.2.1 Model Convergence

The first step to ensure that the FE software is giving reliable answers is to check that results generated converge with mesh refinement. To show this, the four test cases used in section 4 were analysed using varying mesh sizes and the membrane and bending stress recorded. The normalized stress values for the stress extraction points of each test case were then plotted against the respective mesh sizes and showed satisfactory convergence for all four cases. Figures 5.8 and 5.9 shows the plots of the design case which showed the slowest convergence.

An interesting point to note is that convergence takes place both from below and above. This behaviour is normal for the 5β -NT element being used, which has a known characteristic of not converging monotonically from below, as conventional finite elements do.

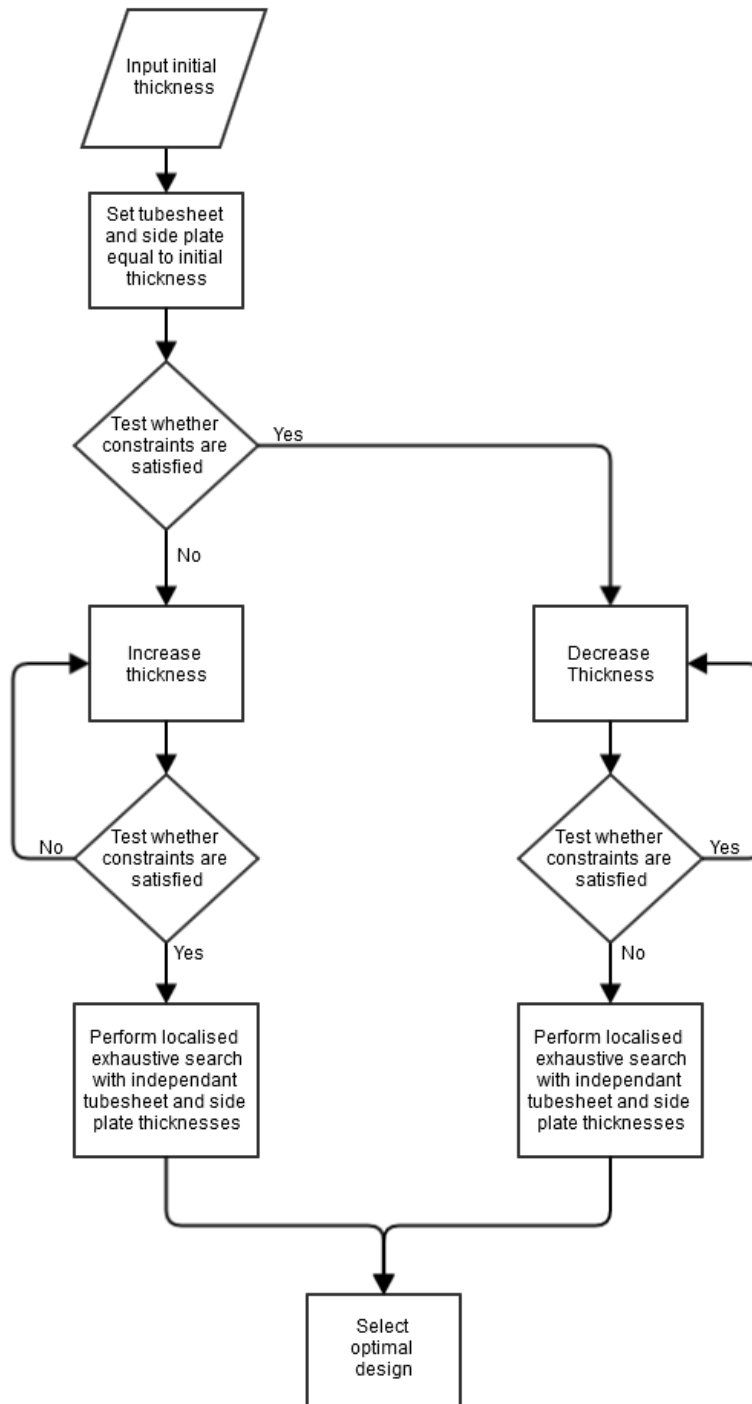


Figure 5.7: Flowchart of Optimisation Search Pattern

The plots for the remaining three cases are given in Appendix D. For all the test cases, the stress values were normalised by dividing the recorded stresses at every extraction point by the stress value recorded for the smallest mesh size at that point. A full record of the actual recorded values are provided in Appendix E.

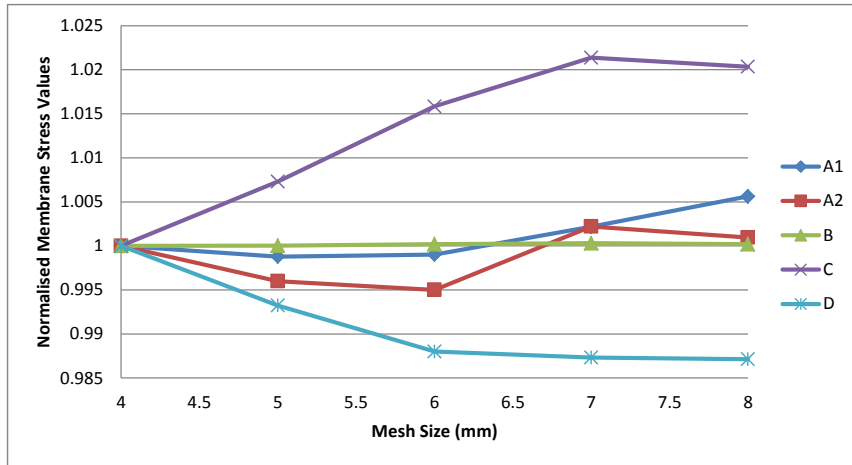


Figure 5.8: Normalised Membrane Stress vs Mesh Size

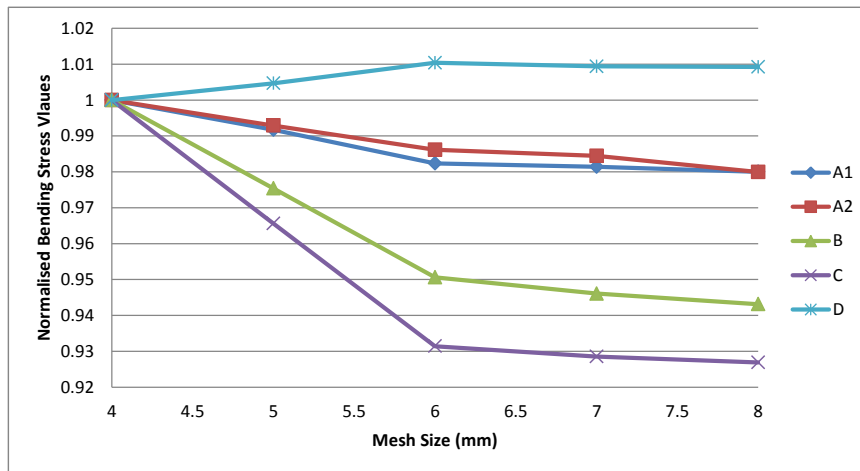


Figure 5.9: Normalised Bending Stress vs Mesh Size

5.2.2 Accuracy Test

In order to confirm that the result generated by the FE software were accurate, they were compared with the MSC.Marc commercial FE package results from chapter 4 in tables 5.3 to 5.5.

The comparison shows a strong correspondence between all the results, with most stress values matching within less than 5% or differing by less than 2 MPa. The only exception to this is at point B for test case 1, where the predicted values differ by 3.1 MPa. Taking into account these results, it is confirmed that the FE software developed for this project yields results that are both reliable and accurate to within industry standards.

Table 5.2: Results Comparison for Test Case 1

	Membrane Stress (MPa)			Bending Stress (MPa)		
	FE	Marc	% Diff	FE	Marc	% Diff
A1	18.7	18.4	2.0	87.3	87.3	0.0
A2	22.5	22.1	2.1	71.1	71.1	0.0
B	8.9	12.0	34.9	121.6	123.1	1.2
C	11.8	11.7	1.3	91.4	95.1	4.0
D	12.6	13.9	10.4	8.6	8.3	3.5

Table 5.3: Results Comparison for Test Case 2

	Membrane Stress (MPa)			Bending Stress (MPa)		
	FE	Marc	% Diff	FE	Marc	% Diff
A1	11.4	11.5	0.9	34.2	34.5	0.9
A2	16.0	16.3	1.4	82.9	83.1	0.2
B	10.0	10.7	7.0	60.8	62.6	3.0
C	10.8	10.7	1.1	51.7	53.9	4.3
D	5.0	5.7	14.4	46.0	45.7	0.7

Table 5.4: Results Comparison for Test Case 3

	Membrane Stress (MPa)			Bending Stress (MPa)		
	FE	Marc	% Diff	FE	Marc	% Diff
A1	11.4	11.2	2.0	29.7	29.9	0.7
A2	16.0	16.3	2.0	66.4	66.4	0.0
B	9.9	10.7	8.2	55.3	57.4	3.8
C	10.4	10.5	0.9	52.8	55.0	4.2
D	5.2	5.9	13.3	43.4	43.1	0.7

Table 5.5: Results Comparison for Test Case 4

	Membrane Stress (MPa)			Bending Stress (MPa)		
	FE	Marc	% Diff	FE	Marc	% Diff
A1	17.4	17.2	1.1	68.4	68.4	0.0
A2	20.0	19.7	1.9	57.2	57.1	0.2
B	8.5	9.8	14.6	92.6	93.4	0.9
C	10.4	10.4	0.0	77.2	78.0	1.0
D	11.1	12.4	11.5	19.7	19.4	1.5

Chapter 6

Overall Results

This chapter will look at the overall impact of the results that have come from this research. First the optimised designs for each of the four test cases will be compared to their initial designs, to quantify the potential for optimisation within the industry. Then, the overall impact of this study will be discussed to access how this research will influence future design methodology.

6.1 Optimisation Potential

After having analysed the original designs of the four test cases from chapter 4, an optimisation was performed on each one to see what their optimal side plate and tubesheet dimensions would be. A comparison of the original and optimised design dimensions is provided in table 6.1. This is followed in table 6.2 by a comparison showing the critical design point and the percentage over design for each of the test cases in their original and optimised state.

Table 6.1: Comparison of Original to Optimised Header Box Designs

Test Case	Side Plate (mm)			Tubesheet (mm)		
	Original	Optimised	% Diff	Original	Optimised	% Diff
1	50	35	30	50	35	30
2	32	20	40	50	35	30
3	30	20	33	45	32	29
4	50	30	40	50	32	36

From these results, we can see that there is a significant savings potential available. The results showed an average savings potential of 36% on side plate materials and 31% on tubesheet material. When these result are put into the context of the header box as a whole, this translate to an average overall material reduction of 18%, as shown by table 6.3

Table 6.2: Comparison of Original to Optimised Designs' Critical Points

Test Case	Original		Optimised	
	Critical Point	% Over Design	Critical Point	% Over Design
1	B	59	B	4
2	D	112	D	1
3	D	122	D	22
4	B	105	B	3

Table 6.3: Overall Material Reduction

Test Case	% Material Reduction
1	20
2	19
3	17
4	16
Average	18

6.2 Research Impact

In its present form the new FE software is not yet developed to the point where it can be used as a primary design tool and its results will still have to be verified and approved by an Authorised Inspection Authority. However, it already allows a designer to remove some uncertainty from the current design environment. In cases where a design has already been influenced by external design factors, such as material and manufacturing factors, the results from the FE software will give a designer the confidence to use the resulting design as is, without adding any further material out of caution. In cases where no external design factor have played a role, the designer can now rely on the accuracy of the FE analysis to either confirm the initial design or use it to adjust the design in any areas where the hand calculations have not been able to capture the true structural behaviour of the header box.

The built in optimiser will also provide the designer with the best design, which will in turn double as the lower safety limit guideline for the header box's design. Additionally, the optimiser will give the designer the capability to modify the major dimensions of a header box and see how this impacts the final optimal design of the tubesheet and side plate, thus promoting better understanding of a header box's structural behaviour and allowing for an interactive design to take place between the various components of the header box.

Chapter 7

Conclusion and Recommendations

7.1 Conclusions

The purpose of this study was to evaluate a method currently used to design cover type heat exchanger header boxes and improve the process to increase its credibility and accuracy.

The first step was to look at how the current design method works. In broad terms it was found that this method simplifies a header box to a collection of simply supported beams, each with a set of representative loads applied to it. Stresses in the header box are then calculated based on this model and compared to a set of failure criteria in order to ensure that the design is adequate.

In order to assess the accuracy of this method, a FE model of a header box was created in order for the results to be compared. First a full 3D FE model was created, but this was subsequently simplified to a representative 2D FE model in order to reduce computational effort and time.

The comparison of these two methods showed that the current design method predicts non-conservative stresses for many parts of a header box. At the same time, the FE results also showed that the header boxes which had been analysed for the comparison were all significantly over designed, even though they had been designed using the current design method. These conflicting results were explained by considering several material, manufacturing and human factors that influence a header box's design, over and above the results from any standard design calculation, which all contribute to its over design.

To solve these problems, it was decided to create a custom 2D FE software package that would automatically set up and analyse a parameterised model of a cover type header box's structure. To this end, a software package was created

that integrates directly with the platform already being used to perform the calculations for the in-house code. An optimiser was also included in the software that takes material and manufacturing constraints into account, in addition to the material failure criteria.

The result is a tool that designers can now use to validate any existing designs as well as provide optimal designs and accurate stress predictions for new header boxes, thus reducing manufacturing costs and reducing uncertainty in the design process.

7.2 Recommendations

At the moment, the 2D FE software tool that was developed is suited for analysing a header box's tubesheet and side plates without nozzles. With further research, this software can be expanded to include three more valuable capabilities.

1. The analysis of the side plate can be expanded to account for the structural behaviour linked to nozzle positioning and size.
2. The program can be upgraded to analyse the remaining components of the header box and show where possible further optimisation can take place in order to further reduce manufacturing costs.
3. The software can be tested further and sufficiently validated so that it can be submitted to ASME to have it approved as an accredited method for designing cover type header boxes.

In its current form the FE model used by the software uses certain assumptions of which the impact should be further investigated.

1. The model assumes that there is no horizontal slip that occurs between the gasket and the side or cover plate. If slip does however occur, it would effect the stress values for the entire structure, but especially those at point A2. Further investigation can be done to confirm whether any slip does take place and if so, what its structural impact will be.
2. The model also uses the assumption that the gasket maintains fixed contact with both the cover and side plate at all times. This will limit the the amount of rotation the structure undergoes around the gasket. Consequently, the model could possibly under predict the true stress values at at points B and C. Further investigation is needed to quantify the structural impact of this assumption and to possibly recommend a more suitable assumption that can be made.

3. Finally, the model does not take into account the loss of material stiffness in the tubesheet due to it being perforated. Instead, only a perforated plate efficiency factor is used to scale up the stresses experienced by the side plate in order to account for the holes. Further investigation is needed to assess the secondary effects that a structurally weakened tubesheet has on the stresses in the side plate.

Appendices

Appendix A

Geometric Details of Test Models

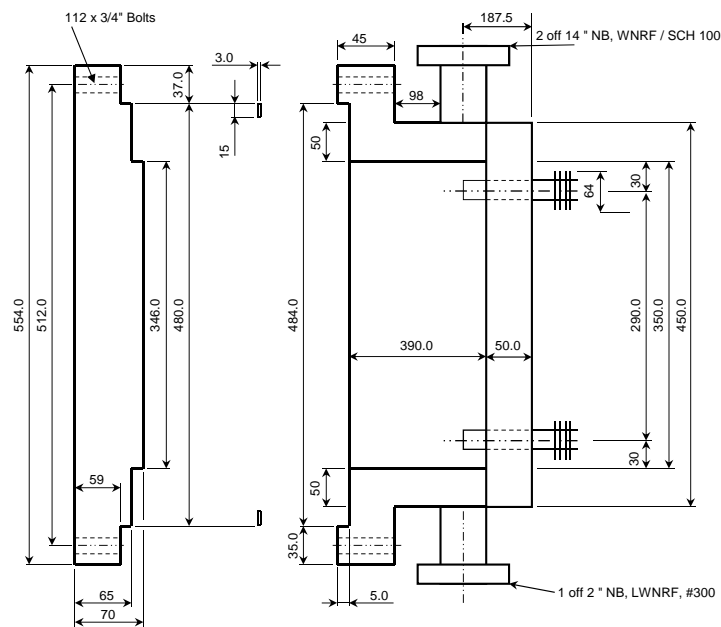


Figure A.1: Test Case 1 Dimensions

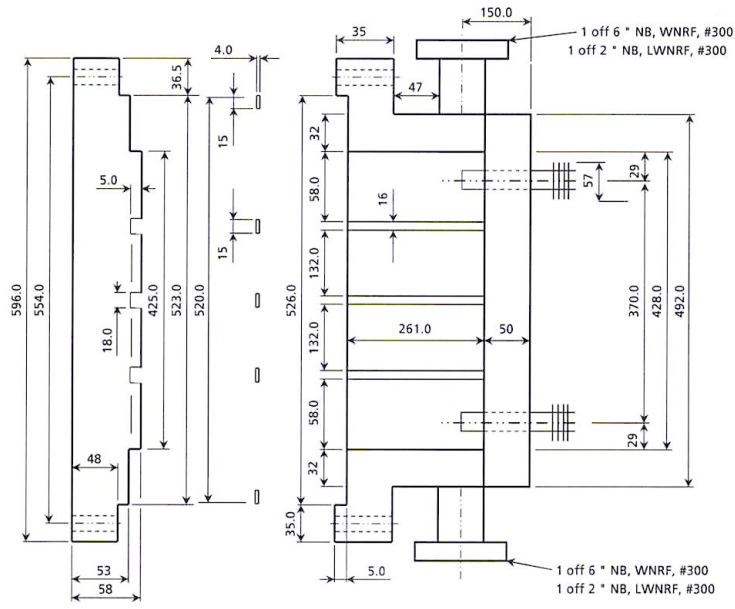


Figure A.2: Test Case 2 Dimensions

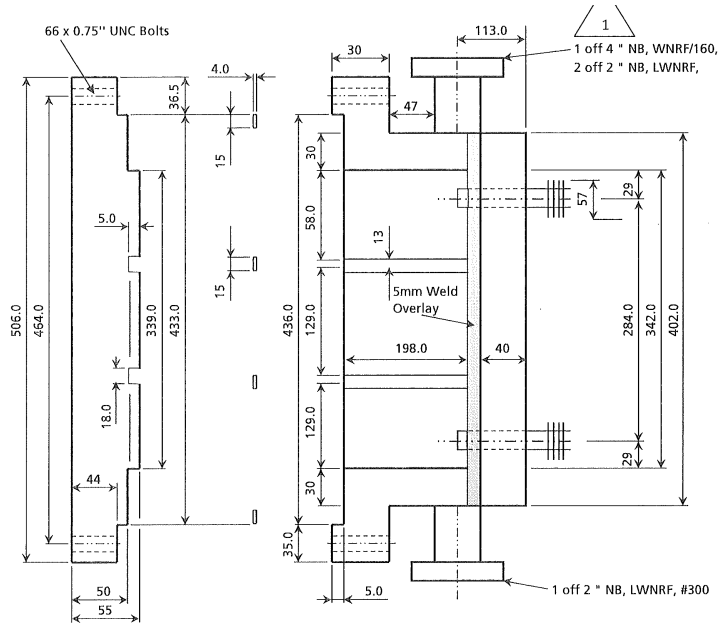


Figure A.3: Test Case 3 Dimensions

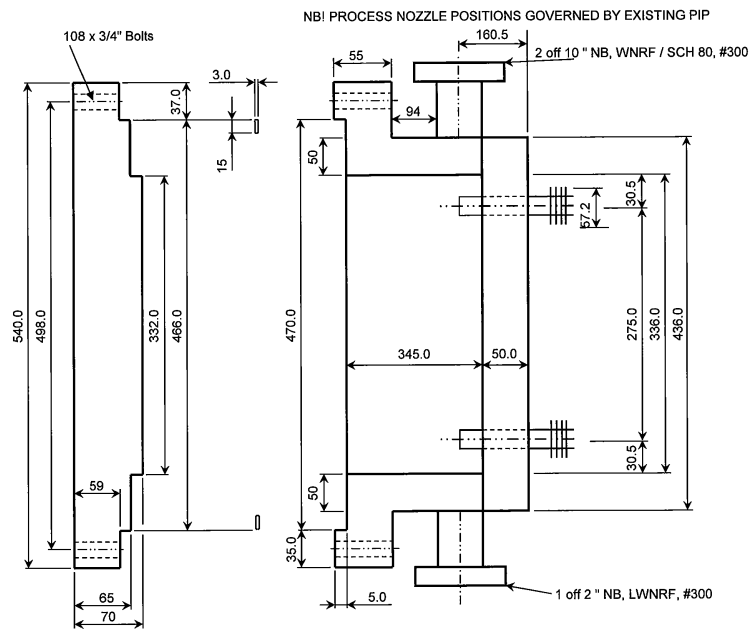


Figure A.4: Test Case 4 Dimensions

Table A.1: Details Regarding Test Cases

Test Case	1	2	3	4
Load Per Bolt (kN)	60.0	30.6	25.5	32.4
Internal Pressure (MPa)	2.50	1.38	1.60	2.50
Design Temperature (°C)	225	208	130	225
Wall Material	SA-516 Grade 70 N	SA-516 Grade 60 N	SA-516 Grade 70 N	SA-516 Grade 70 N

Appendix B

True Stress Strain Material Model

$$\varepsilon_t = \frac{\sigma_t}{E_y} + \gamma_1 + \gamma_2 \quad (\text{B.0.1})$$

$$\gamma_1 = \frac{\varepsilon_1}{2} (1.0 - \tanh[H]) \quad (\text{B.0.2})$$

$$\gamma_2 = \frac{\varepsilon_2}{2} (1.0 - \tanh[H]) \quad (\text{B.0.3})$$

$$\varepsilon_1 = \left(\frac{\sigma_t}{E_y} \right)^{\frac{1}{m_1}} \quad (\text{B.0.4})$$

$$A_1 = \frac{\sigma_{ys} (1 + \varepsilon_{ys})}{(\ln[1 + \varepsilon_{ys}])^{m_1}} \quad (\text{B.0.5})$$

$$m_1 = \frac{\ln[R] + (\varepsilon_p - \varepsilon_{ys})}{\ln \left[\frac{\ln[1 + \varepsilon_p]}{\ln[1 + \varepsilon_{ys}]} \right]} \quad (\text{B.0.6})$$

$$\varepsilon_2 = \left(\frac{\sigma_t}{A_2} \right)^{\frac{1}{m_2}} \quad (\text{B.0.7})$$

$$A_2 = \frac{\sigma_{uts} \exp[m_2]}{m_2^{m_2}} \quad (\text{B.0.8})$$

$$H = \frac{2 [\sigma_t - (\sigma_{ys} + K \{ \sigma_{uts} - \sigma_{ys} \})]}{K (\sigma_{uts} - \sigma_{ys})} \quad (\text{B.0.9})$$

$$R = \frac{\sigma_{ys}}{\sigma_{uts}} \quad (\text{B.0.10})$$

$$\varepsilon_{ys} = 0.002 \quad (\text{B.0.11})$$

$$K = 1.5R^{1.5} - 0.5R^{2.5} - R^{3.5} \quad (\text{B.0.12})$$

$$\sigma_{uts,t} = \sigma_{uts} \exp[m_2] \quad (\text{B.0.13})$$

$$m_2 = 0.60(1.00 - R) \quad (\text{B.0.14})$$

$$\varepsilon_p = 2.0E - 5 \quad (\text{B.0.15})$$

Appendix C

5 β -NT Element Formulation

Stress is calculated using equation C.0.1

$$\sigma = P\beta \quad (\text{C.0.1})$$

Here P is the matrix of element interpolation functions and β is the vector of stress parameters given by

$$\beta = H^{-1}Gq \quad (\text{C.0.2})$$

where q is the nodal displacements and G and H are given by

$$G = \int_{\Omega} P^T B d\Omega \quad (\text{C.0.3})$$

$$H = \int_{\Omega} P_T C^{-1} P d\Omega \quad (\text{C.0.4})$$

Ω is the region of the body being considered and C is the constitutive material relationship.

The nodal displacements q are calculated using

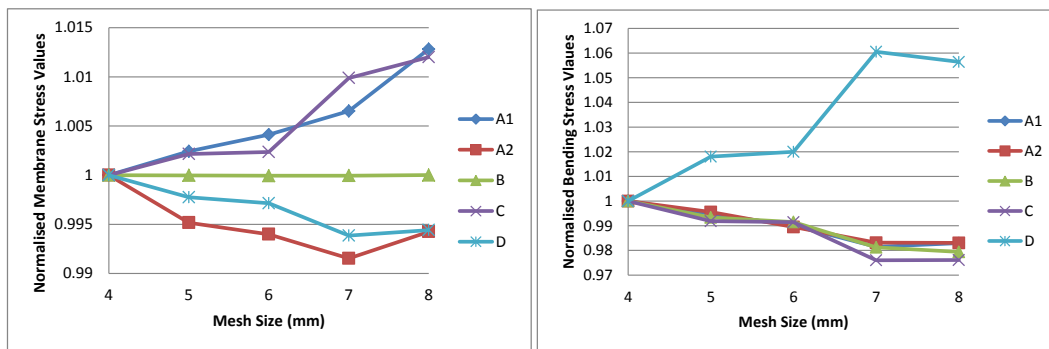
$$q = K^{-1}r \quad (\text{C.0.5})$$

where r is the vector of forces acting on the body and K is the stiffness matrix of the body calculated using equation C.0.6.

$$K = G^T H^{-1} G \quad (\text{C.0.6})$$

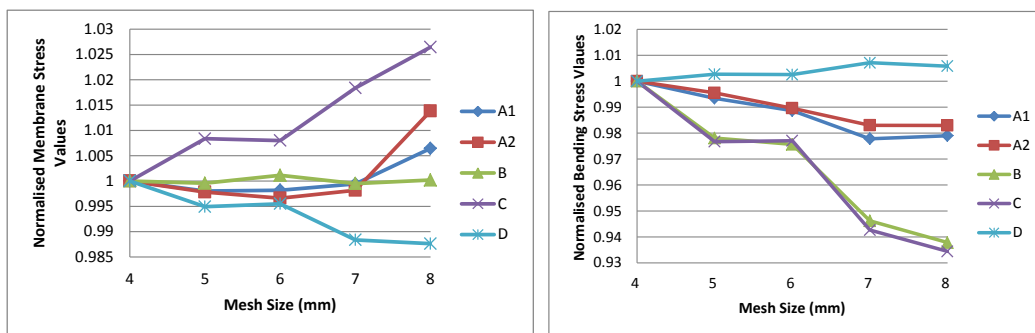
Appendix D

Convergence Test Plots



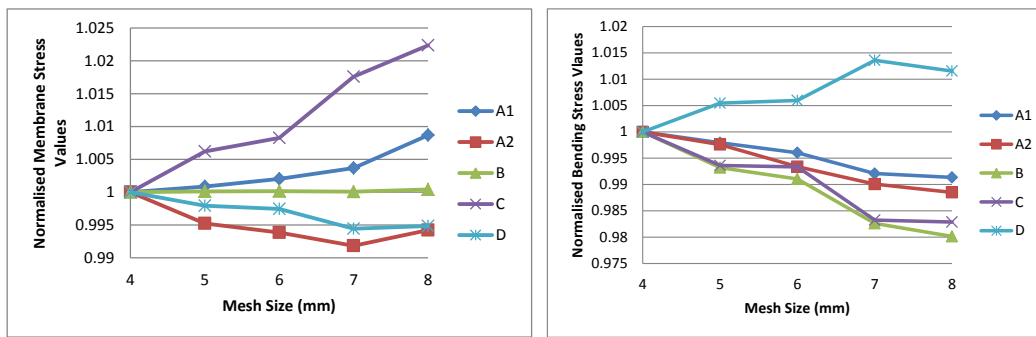
(a) Normalised Membrane Stress vs Mesh size (b) Normalised Bending Stress vs Mesh size

Figure D.1: Test Case 1 Convergence Plots



(a) Normalised Membrane Stress vs Mesh size (b) Normalised Bending Stress vs Mesh size

Figure D.2: Test Case 3 Convergence Plots



(a) Normalised Membrane Stress vs Mesh size (b) Normalised Bending Stress vs Mesh size

Figure D.3: Test Case 4 Convergence Plots

Appendix E

Convergence Test Results

Table E.1: Convergence Test Results for Test Case 1

Mesh Size (mm)	4	5	6	7	8
Membrane Stress (MPa)					
A1	18.7	18.8	18.8	18.9	19.0
A2	22.5	22.4	22.4	22.3	22.4
B	8.9	8.9	8.9	8.9	8.9
C	11.8	11.9	11.9	11.9	12.0
D	12.6	12.6	12.6	12.5	12.5
Bending Stress (MPa)					
A1	87.7	87.6	87.4	87.0	87.0
A2	71.3	71.2	70.9	70.6	70.5
B	122.9	122.1	121.9	120.6	120.4
C	93.4	92.6	92.6	91.1	91.1
D	8.2	8.4	8.4	8.7	8.7

Table E.2: Convergence Test Results for Test Case 2

Mesh Size (mm)	4	5	6	7	8
Membrane Stress (MPa)					
A1	11.4	11.4	11.4	11.4	11.5
A2	16.0	16.0	15.9	16.1	16.0
B	10.0	10.0	10.0	10.0	10.0
C	10.8	10.9	11.0	11.1	11.0
D	5.0	5.0	4.9	4.9	4.9
Bending Stress (MPa)					
A1	34.2	34.0	33.6	33.6	33.6
A2	82.9	82.3	81.8	81.6	81.3
B	60.8	59.3	57.8	57.5	57.3
C	51.7	49.9	48.1	48.0	47.9
D	46.0	46.2	46.5	46.4	46.4

Table E.3: Convergence Test Results for Test Case 3

Mesh Size (mm)	4	5	6	7	8
Membrane Stress (MPa)					
A1	11.4	11.4	11.4	11.4	11.5
A2	16.0	16.0	16.0	16.0	16.2
B	9.9	9.9	9.9	9.9	9.9
C	10.4	10.5	10.5	10.6	10.7
D	5.2	5.2	5.2	5.1	5.1
Bending Stress (MPa)					
A1	29.7	29.5	29.4	29.0	29.1
A2	66.4	66.1	65.7	65.3	65.3
B	55.3	54.1	54.0	52.4	51.9
C	52.8	51.5	51.5	49.7	49.3
D	43.4	43.5	43.5	43.7	43.6

Table E.4: Convergence Test Results for Test Case 4

Mesh Size (mm)	4	5	6	7	8
Membrane Stress (MPa)					
A1	17.4	17.5	17.5	17.5	17.6
A2	20.0	19.9	19.9	19.9	19.9
B	8.5	8.5	8.5	8.5	8.5
C	10.4	10.4	10.5	10.6	10.6
D	11.1	11.1	11.1	11.1	11.1
Bending Stress (MPa)					
A1	68.4	68.3	68.2	67.9	67.8
A2	57.2	57.0	56.8	56.6	56.5
B	92.6	92.0	91.8	91.0	90.8
C	77.2	76.7	76.7	75.9	75.9
D	19.7	19.8	19.8	19.9	19.9

List of References

- Ackers, M.S. (2012). Performance and Thermo-Mechanical Thermo Mechanical Cost Evaluation of API 661 Air-Cooled Air Cooled Heat Exchangers. December, University of Stellenbosch.
- API (2006). Air-Cooled Heat Exchangers for General Refinery Service petrochemical and natural gas industries.
- ASME (2011). Rules for Construction of Pressure Vessels. In: *ASME Boiler & Pressure Vessel Code*, 6th edn. The American Society of Mechanical Engineers, New York.
- Cook, R.D., Malkus, D.S., Plesha, M.E. and Witt, R.J. (2002). *Concepts and Applications of Finite Element Analysis*. 4th edn. John Wiley & Sons, Madison.
- Department of Labour RSA (2009). Pressure Equipment Regulations, Government Gazette 347.
- Di, S. and Ramm, E. (1994). ON ALTERNATIVE HYBRID STRESS 2D AND 3D ELEMENTS. vol. 11, no. December 1992, pp. 49–68.
- EH. Kraamwinkel (2013). Report On Finite Element Analysis performed on the Inlet and Outlet Header Box for the First Compressor Intercooler to Verify the Integrity of Box and Nozzles. Tech. Rep. 217, Axis Mechanical Design (PTY) Ltd.
- GEA Rainey (nd). Air Cooled Heat Exchanger Overview.
Available at: http://www.gearainey.com/opencms/opencms/grc/en/Air_Cooled_Heat_Exchangers/
- Hudson Product Corp. (2009). Basic of Air-cooled Heat Exchangers.
Available at: <http://www.hudsonproducts.com/products/finfan/tech.html>
- Prinsloo, L. (2011). A critical evaluation of the design of removable cover-plate header boxes for air-cooled heat exchangers. April, University of Pretoria.
- SABS (2012). SANS 347 : 2012 SOUTH AFRICAN NATIONAL STANDARD Categorization and conformity assessment criteria for all pressure equipment. p. 25419.
- TEMA (2007). Standards Of The Tubular Exchanger Manufacturers Association.
- Tubetech (nd). TUBETECH air cooled heat exchanger.
Available at: http://www.tubetech.de/sites_en/expert_aircooledhe_en.html